Shallow-water sloshing in rotating vessels undergoing prescribed rigid-body motion in two dimensions — the extended version —

by H. Alemi Ardakani & T. J. Bridges

Department of Mathematics, University of Surrey, Guildford GU2 7XH UK

— October 16, 2010—

Abstract

New shallow-water equations, for sloshing in two dimensions (one horizontal and one vertical) in a vessel which is undergoing rigid-body motion in the plane, are derived. The planar motion of the vessel (pitch-surge-heave or roll-sway-heave) is exactly modelled and the only approximations are in the fluid motion. The flow is assumed to be inviscid but vortical, with approximations on the vertical velocity and acceleration at the surface. These equations improve previous shallow water models for sloshing. The model also contains the essence of the Penney-Price-Taylor theory for the highest standing wave. The surface shallow water equations are simulated using an implicit finite-difference scheme. Numerical experiments are reported, including comparisons with existing results in the literature. The extension to shallow-water flow in three dimensions and the coupled vessel slosh dynamics are also discussed.

Contents

1 Introduction

The theoretical and experimental study of fluid sloshing has a long history and continues to attract considerable attention because of its importance in applications: the shipping of liquid natural gas, sloshing of trapped water on the deck of a ship, liquid transport along roads, as well as unusual applications such as sloshing in a swimming pool on-board a passenger ship (Ruponen et al. [59]), sloshing in a fish tank on deck (Lee et al. [42]), sloshing in automobile fuel tanks (Wiesche [65]), and transport of liquids by robots in industrial applications (Tzamtzi & Kouvakas [63]). Examples where shallow water sloshing is predominant are sloshing of trapped water on the deck of fishing vessels (Caglayan & Storch [16], Adee & Caglayan [4]), and on the deck of offshore supply vessels (Laranjinha et al. [41]), and sloshing in wing fuel tanks of aircraft (Disimile et al. [24]). The recent books of Ibrahim [35] and Faltinsen & Timokha [28] which have over 3000 references are both testimony to the current interest in the subject, and an encyclopedic review of existing research on sloshing.

Although there is a rich history of the study of sloshing, there remains a considerable range of phenomena that are not understood, mainly because sloshing is driven by a free surface motion which is highly nonlinear. In addition there are the attendant problems of fluid-ship interaction, hydroelastic effects, bubble formation, wave breaking and impact, and probabilisitic aspects.

The interest in this paper is in sloshing in shallow water in a vessel that is undergoing a general rigid body motion. In this paper attention is restricted to two dimensions and the case of three dimensions is considered in Alemi Ardakani & Bridges [10]. The aim is to use exact equations for the rigid body motion of the vessel but approximate the equations for the fluid motion. The approximations should simplify the equations but with the minimum number of hypotheses.

The results in the literature on forced (vessel motion prescribed) shallow water sloshing fall into two categories: derive approximate partial differential equations similar to the classical shallow water equations, or use asymptotics, based on small depth aspect ratio and forcing amplitude, to derive approximate equations which can be analyzed more efficiently.

The first example of the former is the work of Verhagen & van Wijngaarden [64]. They write down an approximation of the shallow-water equations of the form

$$h_t + (h\widetilde{u})_x = 0 \quad \text{and} \quad \widetilde{u}_t + \widetilde{u}\widetilde{u}_x + gh_x = \varepsilon \sin \omega t \,, \tag{1.1}$$

where $\varepsilon \sin \omega t$ is due to the imposed rotation of the vessel, $h(x,t)$ is the depth, and $\widetilde{u}(x,t)$ is the horizontal velocity. The tilde is used to distinguish this choice of velocity from other velocities used in this paper. A fixed frame is used so time-dependent boundary conditions are imposed at the endwalls, $x = 0, L$. They solved the equations approximately using a form of the method of characteristics. The principle observation is the formation of a travelling hydraulic jump, and its characteristics were shown to be in agreement with experiments. In followup work by Chester [19], the effect of dispersion and dissipation is included in the shallow water model, showing improved comparison with the experiments of Chester & Bones [20]. Jones & Hulme [37] start with the full equations relative to a rotating frame and give a new derivation of (1.1); they study the equations numerically and with the use of a multi-scale perturbation expansion.

The first work using asymptotics to study forced sloshing in shallow water is Ockendon & Ockendon [50]. The forcing is simplified to a harmonic horizontal translation, and the small parameters are the depth aspect ratio, the amplitude of the forcing and the frequency detuning. Rather than start with the shallow water equations, they start with the full equations for irrotational flow and derive an integrodifferential equation for the surface motion of the form

$$\frac{\widetilde{\kappa}^2}{3}(\eta_{tt}+\eta)-\lambda\eta-\frac{3}{2}\eta^2+\frac{2}{\pi}\cos t=-\frac{3}{2}\int_{-\pi}^{+\pi}\eta(s)^2\,\mathrm{d}s\,, \tag{1.2}$$

where $\widetilde{\kappa}$ and λ are parameters, related to the dispersion and frequency detuning respectively, and $\eta(t)$ is required to be a $2\pi-$periodic function of t. In the limit $\widetilde{\kappa}\to 0$ and $\lambda\to 0$ this equation simplifies to an algebraic equation for η. From this algebraic equation it can be deduced that there are three regions in the frequency-amplitude plane. For fixed amplitude there is an interval around the natural frequency where (the hydraulic analogy of) compressive shocks can be found, and outside this region the solutions are regular periodic standing waves. Experiments of Kobine [39] showed excellent agreement with these results (see Figure 7 of [39]). In further work Ockendon et al. [51] it is shown that this equation has a wide range of exotic solutions. It has since inspired study from a dynamical systems perspective (e.g. [31, 38, 30]). The equation (1.2) has an infinite number of periodic and subharmonic solutions. These works show how forced shallow water sloshing can lead to very complicated fluid motion through a cascade of subharmonic solutions.

The range of validity of the asymptotic approach was extended by Faltinsen & Timokha [27] using modal expansion combined with asymptotics. They examine resonant waves in shallow water (depth to width ratios between $\frac{1}{10}$ and $\frac{1}{4}$) forced by surge & pitch excitation at frequencies in the vicinity of the lowest natural frequency. The principal small parameter is forcing amplitude which is of order ϵ. The depth aspect ratio, velocity potential and wave height are then all required to be of order $\epsilon^{1/4}$. This scaling brings in nonlinearity to fourth order and dispersion. The dispersion gives the theory a modal form of Boussinesq equation, and no additional boundary conditions at the endwalls are required. Secondary resonances are included. This theory allows for large dimension modal expansion and they include up to 20 coupled modes. The large modal system of coupled ODEs is then integrated numerically. They emphasize the role of dissipation and validation by comparison with experiments. They show how modal truncation and choice of dissipation influence the comparison with experiments.

The advantage of asymptotic methods is that detailed studies within the range of validity are possible, leading to fundamental observations, and integration of a system of ODEs will in general be much faster than integration of PDEs. However, the disadvantage is the limited range of validity, requiring the depth aspect ratio, forcing amplitude and frequency all to remain within a certain asymptotic range.

In this paper the first approach will be followed: derive a new model PDE based on the shallow water equations. With this model there are no restrictions on the forcing amplitude or frequency, and the vessel can undertake any rotation and translation, with the full generality of the vessel motion retained. Viscosity is neglected but vorticity is retained in the fluid motion and the only further approximations on the fluid are on the vertical velocity and acceleration – at the free surface only. The retention of vorticity is more important in 3D but still plays a role in 2D. For example Figures 14–15 of Chen [18]

show a non-trivial free surface vorticity for a class of 2D sloshing flows, although viscosity is included in [18].

The key to retaining exact motion of the vessel is to use a body-fitted moving coordinate system. The first work in this direction – in the context of shallow water – is the paper of DILLINGHAM [22]. Starting with the full Euler equations in two-dimensions, a set of shallow water equations for $(h, \overline{u})$, where $h(x,t)$ is the fluid depth and $\overline{u}(x,t)$ is the depth-averaged horizontal velocity,

$$\overline{u} = \frac{1}{h}\int_0^h u(x,y,t)\,\mathrm{d}y\,, \tag{1.3}$$

of the following form, were derived

$$h_t + (h\overline{u})_x = 0 \quad \text{and} \quad \overline{u}_t + \overline{u}\,\overline{u}_x + a(x,t)^D h_x = b(x,t)^D\,, \tag{1.4}$$

where the terms $a(x,t)^D$ and $b(x,t)^D$ contain the vertical and horizontal accelerations of the moving vessel (precise expressions are given in §9). The boundary conditions are $\overline{u} = 0$ at the sidewalls.

With the choice of mean velocity $\overline{u}(x,t)$ the mass equation is exact in (1.4). However, the derivation of the momentum equation requires a number of assumptions. The derivation in DILLINGHAM [22] is somewhat ad hoc, in that terms are neglected without clear implications. A more careful derivation of the equations (1.4) is given by ARMENIO & LA ROCCA [12]. Their derivation leads to an equation of the same form as (1.4) but their coefficients, denoted $a(x,t)^{ALR}$ and $b(x,t;y)^{ALR}$, are very different from those in (1.4). Both derivations will be reviewed in §9.

In constructing a shallow-water approximation, the velocity can be chosen to be the horizontal velocity at any point between the bottom and the surface, or it can be an average velocity. In principle, within the shallow-water approximation, all these velocities should give the same equation, and that is the case – *without rotation*. With rotation, different choices of horizontal velocity lead to different shallow water equations. Our original intention was to use the depth-averaged velocity and precisely itemize the assumptions involved. The depth-averaged velocity seems most natural because the equation $h_t + (h\overline{u})_x = 0$ is then exact.

We discovered however that using the *horizontal surface velocity*,

$$U(x,t) := u(x,y,t)\Big|^h\,, \tag{1.5}$$

where the surface notation is defined by

$$f\Big|^h := f(x,y,t)\Big|_{y=h} = f(x,h(x,t),t)\,, \tag{1.6}$$

leads to equations with some surprising and useful properties.

In two-dimensions (one vertical and one horizontal space direction), consider the inviscid – but retaining vorticity – sloshing problem, with fluid occupying the region $0 < y < h(x,t)$ with $0 \le x \le L$. The governing equations are the Euler equations relative to a moving frame of reference, and conservation of mass, with the usual boundary

conditions (the details are recorded in §2). Remarkably, the horizontal surface velocity satisfies the exact equation

$$U_t + UU_x + \left(a(x,t) + \left.\frac{Dv}{Dt}\right|^h \right) h_x = b(x,t) + \sigma\kappa_{xx}\,, \tag{1.7}$$

where $\left.\frac{Dv}{Dt}\right|^h$ is the Lagrangian vertical acceleration at the free surface, $a(x,t)$ is vertical acceleration due to the rotating frame, and reduces to g, the gravitational constant, when the reference frame is stationary, and $b(x,t)$ is a horizontal acceleration due to the rotating frame (derivation given in §3).

The term $\sigma\kappa_{xx}$ is a curvature term and appears only when surface tension is present, with $\sigma > 0$ the coefficient of surface tension. The curvature term is of the form

$$\sigma\kappa_{xx} = \sigma\, h_{xxx} + \cdots\,,$$

where the dots represent terms nonlinear in h (see equation (6.4)), and so surface tension provides a form of dispersive regularization.

The equation (1.7) is not closed since it requires the vertical acceleration at the surface, but the form is illuminating, and neglect of the Lagrangian vertical acceleration gives a closed system. On the other hand, equation (1.7) shows how the Lagrangian vertical acceleration drives the surface dynamics. In the case where tank is fixed, the acceleration term reduces to

$$a^L := g + \left.\frac{Dv}{Dt}\right|^h .$$

According to early work of Penney & Price [56] and Taylor [62], a^L is precisely the term that drives breaking of standing waves. They argue that $a^L \approx 0$ is the condition for the highest standing wave. Experiments of Taylor [62] confirmed the importance of this quantity. In this paper we will be primarily interested in the case of shallow water where the Lagrangian vertical accelerations at the surface are small, but some comments about the case $a^L \approx 0$ are in Appendix C.

The kinematic condition at the free surface is

$$h_t + Uh_x = V \quad \text{or} \quad h_t + (hU)_x = V + hU_x\,, \tag{1.8}$$

where $V = v(x, h(x,t), t)$ is the vertical velocity at the surface. Hence, it is clear from (1.7) and (1.8) that a closed system of shallow water equations is obtained by making the following assumptions on the vertical velocity and acceleration – at the surface,

$$\left| V + hU_x \right| << U_0\,, \quad \text{and} \quad \left| \left.\frac{Dv}{Dt}\right|^h \right| << |a|\,, \tag{1.9}$$

where U_0 is a reference order one velocity. When the amplitude of rotation is small the second condition requires the magnitude of the vertical acceleration at the surface to be small compared with g.

It is equations (1.7) and (1.8), with the two assumptions (1.9) which are the basis for the analysis and numerics in this paper. This shallow-water model for sloshing is simulated

with an implicit numerical algorithm that is similar to a one-dimensional Abbott-Ionescu scheme. This scheme and its variants are widely used in hydraulics ABBOTT [2]. A review of other schemes that have been or could be used is given in §10. The main reason for using this scheme is that it generalizes nicely to two-horizontal space dimensions and is used in [10]. Secondary reasons include the form of the numerical dissipation generated by the truncation error, the block tridiagonal structure, and its generalization to include dynamic coupling with the vessel motion. The application of this scheme requires only the solution of block tridiagonal coefficient matrices at each step, with an iterative process to account for the nonlinearity.

An outline of the paper is as follows. The governing equations are recorded in §2, based on a new derivation of the moving frame equations in ALEMI ARDAKANI & BRIDGES [11]. In §3 a derivation of the new shallow water slosh equation (1.7) is given. In §9 a detailed comparison of the new SWEs with previous work is presented. The numerical algorithm is then developed in §10. The simulations based on the new algorithm are then presented in §12. The theory and computation in this paper point to new directions for 3D sloshing and for dynamic coupling between the vessel and fluid motion and these directions are discussed in §15.

2 Governing equations

The configuration of the fluid in a rotating-translating vessel is shown in Figure 1. The vessel is a rigid body and two frames of reference are used to study the motion. The spatial (inertial) frame has coordinates $\mathbf{X} = (X, Y)$ and the body frame has coordinates $\mathbf{x} = (x, y)$. The distance from the body frame origin to the point of rotation is denoted by $\mathbf{d} = (d_1, d_2)$ and $\mathbf{d}$ is a constant. The whole system has a uniform translation $\mathbf{q}(t)$. The position of a particle in the body frame is related to a point in the spatial frame by

$$\mathbf{X} = \mathbf{Q}(\mathbf{x} + \mathbf{d}) + \mathbf{q}\,,$$

where $\mathbf{Q}$ is a proper rotation ($\mathbf{Q}^T = \mathbf{Q}^{-1}$ and $\det(\mathbf{Q}) = 1$). The position of the rigid body is uniquely described by the pair $(\mathbf{q}, \mathbf{Q})$ O'REILLY [53]. Let $\theta(t)$ be the angular position between the X and x axes. The angular velocity *vector* is $\mathbf{\Omega} = (0, 0, \Omega)$ with $\Omega = \dot{\theta}$. The connection between θ and $\mathbf{Q}$ is

$$\dot{\mathbf{Q}} = \dot{\theta}\mathbf{J}\mathbf{Q}\,, \quad \mathbf{J} = \begin{pmatrix} 0 & -1 \\ 1 & 0 \end{pmatrix}.$$

The fluid occupies the region

$$0 \le y \le h(x,t) \quad \text{with} \quad 0 \le x \le L\,.$$

The governing equations relative to the body frame will be used. The body (moving) frame for sloshing has been used by a number of authors (e.g. LOU ET AL. [47], FALTINSEN ET AL. [26], LA ROCCA ET AL. [40], IBRAHIM [35], FALTINSEN & TIMOKHA [28]). There are some subtleties, especially in 3D which will be used in [10], and so a new derivation based on first principles is given in the technical report [11]. The momentum equations, derived in [11], for the fluid in the vessel relative to the body coordinate system fixed to

the vessel, are

$$\begin{aligned} \tfrac{Du}{Dt} + \tfrac{1}{\rho}\tfrac{\partial p}{\partial x} &= -g\sin\theta + 2\Omega v + \dot{\Omega}(y+d_2) + \Omega^2(x+d_1) - \ddot{q}_1\cos\theta - \ddot{q}_2\sin\theta\,, \\ \tfrac{Dv}{Dt} + \tfrac{1}{\rho}\tfrac{\partial p}{\partial y} &= -g\cos\theta - 2\Omega u - \dot{\Omega}(x+d_1) + \Omega^2(y+d_2) + \ddot{q}_1\sin\theta - \ddot{q}_2\cos\theta\,, \end{aligned} \tag{2.1}$$

where $g > 0$ is the gravitational constant and

$$\frac{Du}{Dt} := \frac{\partial u}{\partial t} + u\frac{\partial u}{\partial x} + v\frac{\partial u}{\partial y}\,.$$

Conservation of mass relative to the body frame takes the usual form

$$u_x + v_y = 0\,. \tag{2.2}$$

The boundary conditions are

$$u = 0 \quad \text{at} \quad x = 0 \quad \text{and} \quad x = L\,, \quad v = 0 \quad \text{at} \quad y = 0\,, \tag{2.3}$$

and

$$p = -\rho\sigma\kappa_x \quad \text{and} \quad h_t + uh_x = v\,, \quad \text{at} \quad y = h(x,t)\,, \tag{2.4}$$

where $\sigma \geq 0$ is the coefficient of surface tension and

$$\kappa := \frac{h_x}{\sqrt{1+h_x^2}}\,.$$

The vorticity is defined by

$$\mathcal{V} = \frac{\partial v}{\partial x} - \frac{\partial u}{\partial y}\,.$$

The equation governing vorticity is obtained by differentiating the $x-$momentum equation with respect to y and the $y-$momentum equation with respect to x, leading to

$$\frac{D}{Dt}\mathcal{V} = \frac{\partial}{\partial x}\left(\frac{Dv}{Dt}\right) - \frac{\partial}{\partial y}\left(\frac{Du}{Dt}\right) - (u_x + v_y)\mathcal{V} = -2\dot{\Omega}\,, \tag{2.5}$$

with the second equality following from substitution into (2.1) and use of (2.2). This equation is important for the derivation of the shallow water equations. The integrated form of the vorticity equation is

$$\frac{\partial}{\partial t}\left(\int_0^h \mathcal{V}\,\mathrm{d}y\right) + \frac{\partial}{\partial x}\left(\int_0^h u\mathcal{V}\,\mathrm{d}y\right) = -2\dot{\Omega}\,h\,. \tag{2.6}$$

Let

$$\overline{\mathcal{V}} := \int_0^L \int_0^h (\mathcal{V} + 2\Omega)\,\mathrm{d}y\mathrm{d}x\,. \tag{2.7}$$

It follows from (2.6) that $\overline{\mathcal{V}}_t = 0$ and so $\overline{\mathcal{V}}$ is a constant of motion.

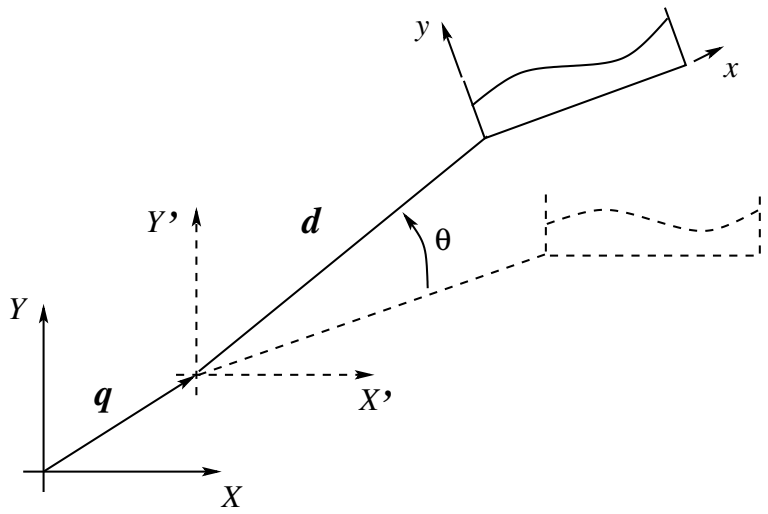

Figure 1: Diagram showing coordinate systems for rotating translating tank. The coordinate system (X', Y') is the translation by $\mathbf{q}$ of the fixed coordinate system (X, Y).

3 Reduction of the pressure gradient

The key to the derivation of the shallow water equations is the treatment of the pressure field. Integrating the vertical momentum equation in (2.1) from any point y to the surface h, and applying the pressure free-surface boundary condition gives the following exact equation for the pressure field,

$$\begin{aligned} \tfrac{1}{\rho}p(x,y,t) &= \int_y^h \frac{Dv}{Dt}ds + 2\Omega\int_y^h u\,ds \\ &\quad +(g\cos\theta + \dot{\Omega}(x+d_1) - \Omega^2 d_2)(h-y) - \frac{1}{2}\Omega^2(h^2-y^2) - \sigma\kappa_x\,, \end{aligned} \tag{3.1}$$

plus the terms associated with $\ddot{\mathbf{q}}$ which don't affect the derivation and can be brought back into the end result.

The typical strategy at this point in the derivation of the SWEs is to drop the vertical acceleration term $\frac{Dv}{Dt}$. However, when we differentiate the pressure with respect to x, and use the vorticity equation, this term simplifies, and so it can be retained exactly.

An expression for the horizontal pressure gradient can be obtained by differentiating the exact expression for the pressure (3.1). Look at the term with the Lagrangian vertical acceleration first, and apply the vorticity equation (2.5)

$$\begin{aligned} \frac{\partial}{\partial x}\left(\int_y^h \frac{Dv}{Dt}ds\right) &= h_x\frac{Dv}{Dt}\bigg|^h + \int_y^h \frac{\partial}{\partial x}\left(\frac{Dv}{Dt}\right)ds \\ &= h_x\frac{Dv}{Dt}\bigg|^h + \int_y^h \left[\frac{\partial}{\partial y}\left(\frac{Du}{Dt}\right) - 2\dot{\Omega}\right]ds \\ &= h_x\frac{Dv}{Dt}\bigg|^h + \frac{Du}{Dt}\bigg|_y^h - 2\dot{\Omega}(h-y). \end{aligned}$$

Now, for the second term

$$\begin{aligned}\frac{\partial}{\partial x}\left(2\Omega\int_y^h u\,ds\right) &= 2\Omega h_x u\Big|^h + 2\Omega\textstyle\int_y^h u_x\,ds \\ &= 2\Omega h_x u\Big|^h + 2\Omega\textstyle\int_y^h (u_x+v_y)\,ds - 2\Omega\int_y^h v_y\,dy \\ &= 2\Omega h_x u\Big|^h - 2\Omega\left(v\Big|^h - v(x,y,t)\right) \\ &= -2\Omega h_t + 2\Omega v(x,y,t)\,.\end{aligned}$$

Using $u_x + v_y = 0$ and the kinematic free surface boundary condition.

Now differentiate the complete expression for $p(x,y,t)$

$$\begin{aligned}\frac{1}{\rho}\frac{\partial p}{\partial x} &= \frac{\partial}{\partial x}\left(\int_y^h \frac{Dv}{Dt}ds\right) + \frac{\partial}{\partial x}\left(2\Omega\int_y^h u\,ds\right) \\ &\quad +\dot\Omega(h-y) + (g\cos\theta + \dot\Omega(x+d_1) - \Omega^2 d_2)h_x - \Omega^2 h h_x - \sigma\kappa_{xx} \\ &= h_x\tfrac{Dv}{Dt}\Big|^h + \tfrac{Du}{Dt}\Big|_y^h - 2\dot\Omega(h-y) - 2\Omega h_t + 2\Omega v \\ &\quad +\dot\Omega(h-y) + (g\cos\theta + \dot\Omega(x+d_1) - \Omega^2 d_2)h_x - \Omega^2 h h_x - \sigma\kappa_{xx} \\ &= h_x\tfrac{Dv}{Dt}\Big|^h + \tfrac{Du}{Dt}\Big|_y^h - \dot\Omega(h-y) - 2\Omega h_t + 2\Omega v \\ &\quad +(g\cos\theta + \dot\Omega(x+d_1) - \Omega^2(h+d_2))h_x - \sigma\kappa_{xx} \\ &= \left(g\cos\theta + \dot\Omega(x+d_1) - \Omega^2(h+d_2) + \tfrac{Dv}{Dt}\Big|^h\right)h_x \\ &\quad +\tfrac{Du}{Dt}\Big|_y^h - \dot\Omega(h-y) - 2\Omega h_t + 2\Omega v - \sigma\kappa_{xx}\,.\end{aligned} \tag{3.2}$$

4 Reduction of the horizontal momentum equation

Now substitute (3.2) into the $x-$momentum equation in (2.1)

$$\begin{aligned}&\frac{Du}{Dt} + \frac{Du}{Dt}\Big|_y^h + \left(g\cos\theta + \dot\Omega(x+d_1) - \Omega^2(h+d_2) + \frac{Dv}{Dt}\Big|^h\right)h_x \\ &\quad -\dot\Omega(h-y) - 2\Omega h_t + 2\Omega v = -g\sin\theta + 2\Omega v + \dot\Omega(y+d_2) + \Omega^2(x+d_1)\,.\end{aligned}$$

There are convenient cancellations: $\frac{Du}{Dt}$, $2\Omega v$ and $\dot\Omega y$ all cancel out, leaving

$$\begin{aligned}&\frac{Du}{Dt}\Big|^h + \left(g\cos\theta + \dot\Omega(x+d_1) - \Omega^2(h+d_2) + \frac{Dv}{Dt}\Big|^h\right)h_x \\ &\qquad = 2\Omega h_t - g\sin\theta + \dot\Omega(h+d_2) + \Omega^2(x+d_1) + \sigma\kappa_{xx}\,.\end{aligned} \tag{4.1}$$

Conveniently, the material derivative of u at the surface can be expressed purely in terms of the surface horizontal velocity

$$U_t + UU_x = [u_t + u_y h_t + uu_x + uu_y h_x]\Big|^h = \tfrac{Du}{Dt}\Big|^h + u_y(h_t + uh_x - v)\Big|^h = \tfrac{Du}{Dt}\Big|^h .$$

Substituting into (4.1) then gives the $x-$momentum equation at the free surface

$$U_t + UU_x + \left(a(x,t) + \tfrac{Dv}{Dt}\Big|^h \right) h_x = b(x,t) + \sigma\kappa_{xx} \,, \tag{4.2}$$

where, after adding back in the terms with $\ddot{q}_1$ and $\ddot{q}_2$,

$$\begin{aligned} a(x,t) &= g\cos\theta + \dot{\Omega}(x+d_1) - \Omega^2(h+d_2) - \ddot{q}_1\sin\theta + \ddot{q}_2\cos\theta \\ b(x,t) &= 2\Omega h_t - g\sin\theta + \dot{\Omega}(h+d_2) + \Omega^2(x+d_1) - \ddot{q}_1\cos\theta - \ddot{q}_2\sin\theta \,. \end{aligned} \tag{4.3}$$

The equation (4.2) is exact. Note also that the assumption of finite-depth is never used in the derivation of (4.2). It is also valid for an infinite-depth fluid. The translation vector (q_1, q_2) is relative to the spatial frame. The rotation of the acceleration vector $(\ddot{q}_1, \ddot{q}_2)$ that appears in (4.3) is due to the fact that these accelerations are viewed from the body frame in (4.2). When the vessel is stationary (4.2) reduces to the surface equation for the classical water wave problem (cf. Bridges [15]).

There is also an exact equation for the surface vorticity. Let

$$\Gamma(x,t) := \mathcal{V}\Big|^h := (v_x - u_y)\Big|^h \,.$$

Then evaluating (2.5) at $y = h$,

$$\Gamma_t + U\Gamma_x = -2\dot{\Omega} \,.$$

Hence $\Gamma + 2\Omega$ is transported by the horizontal surface velocity. However, in contrast to conservation of $\overline{\mathcal{V}}$ in (2.7), conservation of *surface* vorticity is nullified in general by the boundary conditions

$$\frac{d}{dt}\left(\int_0^L \Gamma \,\mathrm{d}x + 2L\Omega \right) = \int_0^L \Gamma U_x \,\mathrm{d}x \,.$$

5 Conservation of mass

The vertical average of the horizontal velocity $\overline{u}(x,t)$ is defined by

$$\overline{u}(x,t) := \tfrac{1}{h}\textstyle\int_0^h u(x,y,t)\mathrm{d}y \,.$$

Differentiating

$$\begin{aligned} h_t + (h\overline{u})_x &= h_t + h_x u\Big|^h + \textstyle\int_0^h u_x \mathrm{d}y \\ &= h_t + Uh_x + \textstyle\int_0^h (u_x + v_y)\,\mathrm{d}y - \int_0^h v_y \mathrm{d}y \\ &= h_t + Uh_x - V + v\Big|_{y=0} \\ &= 0 \,, \end{aligned}$$

using $u_x+v_y=0$, the bottom boundary condition and the kinematic free surface boundary condition. Hence if $\overline{u}$ is used for the horizontal velocity then the $h-$equation in the SWEs in the form

$$h_t + (h\overline{u})_x \;=\; 0\,,$$

is exact.

However as the momentum equation is written in terms of the surface velocity $U(x,t)$, the $h-$equation should also be in terms of the surface velocity. The surface and average velocities are related by

$$U(x,t) - \overline{u}(x,t) \;=\; \tfrac{1}{h}\textstyle\int_0^h yu_y \mathrm{d}y\,. \tag{5.1}$$

Use this identity to formulate the mass equation in terms of the surface velocity field. Differentiating (5.1) and using mass conservation,

$$\frac{\partial}{\partial x}\left[h\left(U-\overline{u}\right)\right] = V + hU_x = h_t + (hU)_x\,. \tag{5.2}$$

The error in using the surface velocity $U(x,t)$ in the $h-$equation can be characterized two ways:

$$\left|V + hU_x\right| \ll U_0 \quad \text{or} \quad \left|\tfrac{\partial}{\partial x}\left(h\left(U-\overline{u}\right)\right)\right| \ll U_0\,, \tag{5.3}$$

where U_0 is a reference order one velocity.

6 SWEs for 2-D sloshing in a rotating vessel

To summarize, the pre-SWEs for (h,U) are

$$\begin{aligned} h_t + (hU)_x \;&=\; V + hU_x\,, \\ U_t + UU_x + \left(a(x,t) + \tfrac{Dv}{Dt}\Big|^h\right) h_x \;&=\; b(x,t) + \sigma\kappa_{xx}\,. \end{aligned} \tag{6.1}$$

The equation for $V\,(x,t)$ can be added

$$V_t + UV_x = \frac{Dv}{Dt}\Big|^h\,. \tag{6.2}$$

The system (6.1) with or without (6.2) is not closed. If $\frac{Dv}{Dt}\Big|^h$ is specified, then the system of three equations (6.1)–(6.2) for (h,U,V) is closed. This system of three equations can be further reduced to a system of two equations with an additional assumption on the surface vertical velocity.

Henceforth it is assumed that the vertical velocity at the free surface satisfies

$$\left|V + hU_x\right| \ll U_0\,, \tag{**SWE-1**}$$

and the Lagrangian vertical acceleration at the free surface satisfies

$$\left| \frac{Dv}{Dt} \Big|^h \right| \ll \left| a\left(x,t\right) \right| . \qquad \textbf{(SWE-2)}$$

The assumption (**SWE-1**) has an alternative characterization as shown in (5.3). For non-rotating tank, the second assumption (**SWE-2**) is equivalent to assuming that the Lagrangian vertical acceleration is small compared with the gravitational acceleration

$$\left| \frac{Dv}{Dt} \Big|^h \right| \ll g .$$

Note that the coefficient of h_x in (6.1) can lead to instability and loss of well-posedness. Consider the linearized constant coefficient problem

$$\begin{aligned} h_t + h_0 U_x &= 0 , \\ U_t + \widetilde{a} h_x &= 0 , \end{aligned}$$

where $\widetilde{a}$ is a constant. Differentiating and combining gives the following wave equation

$$h_{tt} - \widetilde{a} h_0 h_{xx} = 0 .$$

This equation is well-posed only when $\widetilde{a} > 0$. So in order that (6.1) with the assumptions (**SWE-1**) and (**SWE-2**) be well-posed, the third assumption is

$$a\left(x,t\right) > 0 . \qquad \textbf{(SWE-3)}$$

Under these assumptions the shallow water equations for sloshing relative to a rotating frame are

$$h_t + (hU)_x = 0 \quad \text{and} \quad U_t + UU_x + a(x,t)h_x = b(x,t) + \sigma \kappa_{xx} , \tag{6.3}$$

with $a(x,t)$ and $b(x,t)$ as defined in equation (4.3). The term $\sigma\kappa_{xx}$ provides dispersive regularization since

$$\kappa_{xx} = \frac{\partial^2}{\partial x^2} \left(\frac{h_x}{\sqrt{1+h_x^2}} \right) = \frac{\partial}{\partial x} \left(\frac{h_{xx}}{(1+h_x^2)^{3/2}} \right) = h_{xxx} + \cdots , \tag{6.4}$$

where the $\cdots$ are nonlinear terms. The term $\sigma\kappa_{xx}$ contributes dispersive regularization at the linear level, much like a Boussinesq term. The equations with $\sigma \neq 0$ have third-order space derivatives and so additional boundary conditions at $x = 0, L$ would be required (Billingham [14]). The primary interest in this paper is long waves, and so surface tension effects will be henceforth neglected

$$\sigma = 0 . \qquad \textbf{(SWE-4)}$$

6.1 Conservation form of the surface SWEs

Surprisingly, even though the coefficients depend on space and time, these equations can be put into conservation form. With $\sigma = 0$ the pair of equations (6.3) is equivalent to

$$\tfrac{\partial}{\partial t}\left(\nabla I\right) + \tfrac{\partial}{\partial x}\left(\nabla E\right) = 0\,, \tag{6.5}$$

with

$$I(h,U) = hU - \Omega(h+d_2)^2\,, \tag{6.6}$$

and

$$\begin{aligned} E \;=\; & \tfrac{1}{2}U^2h + \tfrac{1}{2}g(h+d_2)^2\cos\theta + gxh\sin\theta + \tfrac{1}{2}\dot{\Omega}(x+d_1)(h+d_2)^2 \\ & -\tfrac{1}{6}\Omega^2(h+d_2)^3 - \tfrac{1}{2}h\Omega^2(x+d_1)^2 \\ & -\tfrac{1}{2}(\ddot{q}_1\sin\theta - \ddot{q}_2\cos\theta)(h+d_2)^2 + (\ddot{q}_1\cos\theta + \ddot{q}_2\sin\theta)xh\,. \end{aligned} \tag{6.7}$$

The gradient in (6.5) is with respect to h and U: $\nabla I := \left(\frac{\partial I}{\partial h}, \frac{\partial I}{\partial U}\right)$. The functional I is a generalization of momentum of the SWEs, hU, and E is a generalization of the energy of the SWEs, $\frac{1}{2}hU^2 + \frac{1}{2}gh^2$. A derivation of this conservation form is given in Appendix A.

6.2 Criticality

The form of the equations (6.3) suggests a generalization of criticality. Criticality occurs when the Jacobian of the quasilinear part of (6.3) is singular,

$$\det\begin{bmatrix} U & h \\ a(x,t) & U \end{bmatrix} = 0\,.$$

When the vessel is stationary, the determinant reduces to

$$\det\begin{bmatrix} U & h \\ g & U \end{bmatrix} = gh\left(F^2 - 1\right)\,,$$

where $F^2 = U^2/gh$ is the Froude number; that is, criticality corresponds to the usual case of Froude number unity. When the vessel is undergoing forced translation and/or rotation, the determinant equal to zero gives the condition

$$F^2 = \cos\theta + \frac{\dot{\Omega}}{g}(x+d_1) - \frac{\Omega^2}{g}(h+d_2) - \frac{\ddot{q}_1}{g}\sin\theta + \frac{\ddot{q}_2}{g}\cos\theta\,. \tag{6.8}$$

When the vessel is rotating and or translating, the system can pass through criticality at particular values of x and t. Numerical experiments show that the right hand side of (6.8) can exceed unity (see Figure 14).

7 (SWE-1) and (SWE-2) in the shallow-water limit

In this section a scaling argument and asymptotics are used to analyze (**SWE-1**) and (**SWE-2**) in the shallow-water limit. The *shallowness* parameter is

$$\varepsilon = \frac{h_0}{L}\,,$$

where L is a representative horizontal length scale. Let $U_0 = \sqrt{gh_0}$ be the representative horizontal velocity scale. Introduce the standard shallow-water scaling (e.g. p. 482 of DINGEMANS [23] or p. 26 of JOHNSON [36]),

$$\begin{aligned} \widetilde{x} &= \frac{x}{L}\,, \quad \widetilde{y} = \frac{y}{h_0} = \frac{y}{\varepsilon L}\,, \quad \widetilde{t} = \frac{tU_0}{L}\,, \\ \widetilde{u} &= \frac{u}{U_0}\,, \quad \widetilde{v} = \frac{v}{\varepsilon U_0}\,, \quad \widetilde{h} = \frac{h}{h_0}\,, \quad \widetilde{p} = \frac{p}{\rho g h_0}\,. \end{aligned} \tag{7.1}$$

The scaled version of the surface velocities are denoted by $\widetilde{U}$ and $\widetilde{V}$.

The typical strategy for deriving an asymptotic shallow-water model is to scale the full Euler equations, and then use an asymptotic argument to reduce the vertical pressure field and vertical velocities (e.g. §5.1 of DINGEMANS [23]). Here however we have an advantage as the full Euler equations have been reduced to the exact surface equations (6.1). Hence the strategy here is to start by scaling the exact equations (6.1), and then apply an asymptotic argument. This strategy leads to a concise argument for the shallow-asymptotic form for (**SWE-1**) and (**SWE-2**).

To check (**SWE-1**), start by scaling the exact mass equation in (6.1)

$$\widetilde{h}_{\widetilde{t}} + (\widetilde{h}\widetilde{U})_{\widetilde{x}} = \widetilde{V} + \widetilde{h}\widetilde{U}_{\widetilde{x}}\,. \tag{7.2}$$

At first glance it appears that the left-hand side and the right-hand side are of the same order, since ε does not appear. However, the *sum* of the two terms on the right-hand side is of higher order. The fact that the right-hand side is of higher order is intuitively clear, since it can be expressed in terms of the velocity differences $U - \overline{u}$ and in the shallow-water approximation the horizontal surface velocity and average velocity are asymptotically equivalent. However, to make this precise go back to the unscaled mass equation and rewrite the right-hand side as

$$h_t + (hU)_x = \frac{\partial}{\partial x}\left(\int_0^h y u_y \,\mathrm{d}y\right)\,,$$

using (5.1) and (5.2). Now substitute for u_y using the vorticity field

$$h_t + (hU)_x = \frac{\partial}{\partial x}\left(\int_0^h y\,(v_x - \mathcal{V})\,\mathrm{d}y\right)\,. \tag{7.3}$$

The key to showing the right-hand side is of higher order is the scaling of the vorticity. The appropriate scaling (which leads to a uniform ε^2 estimate of u_y) is to assume that the vorticity is of order ε

$$\mathcal{V} = \frac{U_0}{L}\varepsilon\widetilde{\mathcal{V}}\,.$$

Scaling (7.3) then gives

$$\widetilde{h}_{\widetilde{t}} + (\widetilde{h}\widetilde{U})_{\widetilde{x}} = \varepsilon^2 \frac{\partial}{\partial \widetilde{x}} \int_0^{\widetilde{h}} \widetilde{y}\left(\frac{\partial \widetilde{v}}{\partial \widetilde{x}} - \widetilde{\mathcal{V}}\right)\,\mathrm{d}\widetilde{y}\,. \tag{7.4}$$

Taking the limit $\varepsilon \to 0$ shows that (**SWE-1**) is satisfied. However, to be precise it is essential that

$$\frac{\partial}{\partial \widetilde{x}} \int_0^{\widetilde{h}} \widetilde{y}\left(\frac{\partial \widetilde{v}}{\partial \widetilde{x}} - \widetilde{\mathcal{V}}\right)\,\mathrm{d}\widetilde{y} \quad \text{is bounded in the limit } \varepsilon \to 0\,. \tag{7.5}$$

Assumption (**SWE-2**) requires that the vertical acceleration, $\frac{Dv}{Dt}\Big|^h$, in

$$\left(a(x,t) + \frac{Dv}{Dt}\Big|^h \right) \tag{7.6}$$

be small, relative to magnitude of $a\,(x,t)$. Scaling the Lagrangian vertical acceleration gives

$$\begin{aligned} \frac{Dv}{Dt}\Big|^h &= V_t + UV_x \\ &= \varepsilon \tfrac{U_0^2}{L} \left(\widetilde{V}_{\widetilde{t}} + \widetilde{U}\widetilde{V}_{\widetilde{x}} \right) \\ &= \varepsilon \tfrac{U_0^2}{L} \frac{D\widetilde{v}}{D\widetilde{t}}\Big|^{\widetilde{h}} . \end{aligned}$$

Hence

$$\frac{Dv}{Dt}\Big|^h = g\varepsilon^2 \frac{D\widetilde{v}}{D\widetilde{t}}\Big|^{\widetilde{h}} ,$$

using $U_0^2 = gh_0 = gL\varepsilon$. The scaled version of (7.6) is therefore

$$\left(a + \frac{Dv}{Dt}\Big|^h \right) = g \left(\frac{a}{g} + \varepsilon^2 \frac{D\widetilde{w}}{D\widetilde{t}}\Big|^{\widetilde{h}} \right) .$$

In the shallow-water regime, the assumption (**SWE-2**) is satisfied if

$$\frac{a}{g} \quad \text{is of order one and} \quad \left| \frac{D\widetilde{v}}{D\widetilde{t}}\Big|^{\widetilde{h}} \right| \quad \text{is bounded as} \quad \varepsilon \to 0\,. \tag{7.7}$$

However, by introducing scaling and taking an asymptotic limit, other anomalies can be introduced. Introduce the following scaled variables/parameters

$$\widetilde{q}_1 = \frac{q_1}{L}\,, \quad \widetilde{q}_2 = \frac{q_2}{h_0}\,, \quad \widetilde{d}_1 = \frac{d_1}{L}\,, \quad \widetilde{d}_2 = \frac{d_2}{h_0}\,. \tag{7.8}$$

Now using (7.1) and (7.8) and scaling the momentum equation in (6.3) considering (**SWE-4**) and taking an asymptotic limit as $\varepsilon \to 0$ gives

$$\widetilde{U}_{\widetilde{t}} + \widetilde{U}\widetilde{U}_{\widetilde{x}} + \cos\theta \widetilde{h}_{\widetilde{x}} = -\frac{\sin\theta}{\varepsilon} + \theta_{\widetilde{t}}^2 \left(\widetilde{x} + \widetilde{d}_1 \right) - \widetilde{q}_{1_{\widetilde{t}\widetilde{t}}} \cos\theta\,, \tag{7.9}$$

which shows that the first term on the right-hand side is of order ε^{-1} and is unbounded as $\varepsilon \to 0$. Hence this scaling puts a restriction on the vessel rotation angle. So in the shallow-water regime θ should be of order ε or higher to ensure that the first term on the right-hand side of (7.9) is consistent. In conclusion, this scaling suggest that roll/pitch motion should be an order of magnitude smaller than **q**-translations in order to avoid large fluid motions that would violate (**SWE-1**) and (**SWE-2**).

8 Deriving the rotating SWEs using an asymptotic argument

In this section it is shown that equations (7.4) and (7.9) which are respectively the scaled versions of the new SWEs in (6.1) can be recovered exactly by the classical small parameter argument, starting with the full Euler equations, that is found in most books (e.g. §2.6 of JOHNSON [36]).

Use the standard shallow water scaling introduced in (7.1) and (7.8) and nondimensionalize the Euler equations in (2.1) to obtain respectively the scaled $x-$momentum and $y-$momentum equations

$$\begin{aligned} \widetilde{u}_{\widetilde{t}} + \widetilde{u}\widetilde{u}_{\widetilde{x}} + \widetilde{v}\widetilde{u}_{\widetilde{y}} + \widetilde{p}_{\widetilde{x}} &= -\tfrac{\sin\theta}{\varepsilon} + 2\varepsilon\theta_{\widetilde{t}}\widetilde{v} + \varepsilon\theta_{\widetilde{t}\widetilde{t}}\left(\widetilde{y} + \widetilde{d}_2\right) \\ &\quad + \theta_{\widetilde{t}}^2\left(\widetilde{x} + \widetilde{d}_1\right) - \widetilde{q}_{1_{\widetilde{t}\widetilde{t}}}\cos\theta - \varepsilon\widetilde{q}_{2_{\widetilde{t}\widetilde{t}}}\sin\theta\,, \end{aligned} \tag{8.1}$$

and

$$\begin{aligned} \varepsilon^2\left(\widetilde{v}_{\widetilde{t}} + \widetilde{u}\widetilde{v}_{\widetilde{x}} + \widetilde{v}\widetilde{v}_{\widetilde{y}}\right) + \widetilde{p}_{\widetilde{y}} &= -\cos\theta + \varepsilon\left(-2\theta_{\widetilde{t}}\widetilde{u} - \theta_{\widetilde{t}\widetilde{t}}\left(\widetilde{x} + \widetilde{d}_1\right) + \widetilde{q}_{1_{\widetilde{t}\widetilde{t}}}\sin\theta\right) \\ &\quad + \varepsilon^2\left(\theta_{\widetilde{t}}^2\left(\widetilde{y} + \widetilde{d}_2\right) - \widetilde{q}_{2_{\widetilde{t}\widetilde{t}}}\cos\theta\right)\,. \end{aligned} \tag{8.2}$$

The mass equation scales as

$$\widetilde{u}_{\widetilde{x}} + \widetilde{v}_{\widetilde{y}} = 0\,, \tag{8.3}$$

and the boundary conditions are

$$\widetilde{u} = 0 \quad \text{at} \quad \widetilde{x} = 0 \quad \text{and} \quad \widetilde{x} = 1\,, \quad \widetilde{v} = 0 \quad \text{at} \quad \widetilde{y} = 0\,, \tag{8.4}$$

and

$$\widetilde{p} = 0 \quad \text{and} \quad \widetilde{h}_{\widetilde{t}} + \widetilde{u}\widetilde{h}_{\widetilde{x}} = \widetilde{v}\,, \quad \text{at} \quad \widetilde{y} = \widetilde{h}\left(\widetilde{x}, \widetilde{t}\right)\,, \tag{8.5}$$

where the surface tension is neglected in the boundary condition for pressure.

Taking the limit of as $\varepsilon \to 0$ in (8.2) gives

$$\frac{\partial\widetilde{p}}{\partial\widetilde{y}} = -\cos\theta\,,$$

and so

$$\int_{\widetilde{y}}^{\widetilde{h}} \frac{\partial\widetilde{p}}{\partial\widetilde{y}}\mathrm{d}\widetilde{s} = \int_{\widetilde{y}}^{\widetilde{h}} -\cos\theta\mathrm{d}\widetilde{s}\,, \quad \Rightarrow \quad \widetilde{p}\left(\widetilde{x}, \widetilde{y}, \widetilde{t}\right) = \cos\theta\left(\widetilde{h} - \widetilde{y}\right)\,,$$

using the pressure free surface boundary condition. So the horizontal pressure gradient reads

$$\frac{\partial\widetilde{p}}{\partial\widetilde{x}} = \cos\theta\frac{\partial\widetilde{h}}{\partial\widetilde{x}}\,. \tag{8.6}$$

The vorticity equation is important in deriving the shallow-water equations. Scaling the vorticity equation, $\mathcal{V} = v_x - u_y$, gives

$$\widetilde{u}_{\widetilde{y}} = \varepsilon^2\widetilde{v}_{\widetilde{x}} - \frac{L}{U_0}\varepsilon\mathcal{V}\,.$$

Hence, if $\frac{L}{U_0}\mathcal{V} = \varepsilon^{\mathcal{P}}\widetilde{\mathcal{V}}$ for any $\mathcal{P} \geq 0$ then

$$\widetilde{u}_{\widetilde{y}} = \varepsilon^2 \widetilde{v}_{\widetilde{x}} - \varepsilon^{\mathcal{P}+1}\widetilde{\mathcal{V}} \quad \Rightarrow \quad \widetilde{u}_{\widetilde{y}} \to 0 \quad \text{as} \quad \varepsilon \to 0\,. \tag{8.7}$$

So in the shallow-water limit, the horizontal velocity is independent of y. This is the usual assumption in shallow-water theory.

Now taking the limit of (8.1) as $\varepsilon \to 0$ using (8.6) and (8.7) gives

$$\widetilde{u}_{\widetilde{t}} + \widetilde{u}\widetilde{u}_{\widetilde{x}} + \cos\theta \widetilde{h}_{\widetilde{x}} = -\frac{\sin\theta}{\varepsilon} + \theta_{\widetilde{t}}^2\left(\widetilde{x} + \widetilde{d}_1\right) - \widetilde{q}_{1_{\widetilde{t}\widetilde{t}}}\cos\theta\,,$$

which is exactly the same as (7.9). Now, assuming that

$$\theta = \varepsilon\widetilde{\theta}\,, \tag{8.8}$$

with $\widetilde{\theta}$ of order one, then

$$\frac{\sin\left(\varepsilon\widetilde{\theta}\right)}{\varepsilon} \to \widetilde{\theta} \quad \text{as} \quad \varepsilon \to 0\,.$$

And so this latter equation reduces to

$$\widetilde{u}_{\widetilde{t}} + \widetilde{u}\widetilde{u}_{\widetilde{x}} + \widetilde{h}_{\widetilde{x}} \;=\; -\widetilde{\theta} - \widetilde{q}_{1_{\widetilde{t}\widetilde{t}}}\,, \tag{8.9}$$

noting that in (8.9), $\widetilde{u}$ can be interpreted as the horizontal depth-averaged scaled velocity (see below) and in (7.9), $\widetilde{U}$ is the horizontal surface scaled velocity.

To recover (7.4) integrate equation (8.3) from $\widetilde{y} = 0$ to $\widetilde{y} = \widetilde{h}$,

$$\begin{aligned} 0 &= \int_0^{\widetilde{h}} \left(\widetilde{u}_{\widetilde{x}} + \widetilde{v}_{\widetilde{y}}\right) \mathrm{d}\widetilde{y} \\ &= \widetilde{h}\widetilde{u}_{\widetilde{x}} + \widetilde{v}\Big|^{\widetilde{h}} \\ &= \widetilde{h}_{\widetilde{t}} + \left(\widetilde{h}\widetilde{u}\right)_{\widetilde{x}}\,, \end{aligned} \tag{8.10}$$

using the bottom boundary condition and kinematic free surface boundary condition. Note that in the first line of (8.10), $\widetilde{u}$ in $\widetilde{h}\widetilde{u}_{\widetilde{x}}$ is the horizontal velocity at any level, and in substitution for $\widetilde{v}\big|^{\widetilde{h}}$ from (8.5), $\widetilde{u}$ is the horizontal velocity at the free surface, but as $\widetilde{u}$ is independent of $\widetilde{y}$ the terms on the right-hand side of (8.10) can be summed as in the second line of (8.10). The vertical average of the horizontal scaled velocity is defined by

$$\overline{\widetilde{u}} = \frac{1}{\widetilde{h}}\int_0^{\widetilde{h}} \widetilde{u}\left(\widetilde{x}, \widetilde{y}, \widetilde{t}\right) \mathrm{d}\widetilde{y}\,.$$

Differentiating

$$\begin{aligned} \left(\widetilde{h}\overline{\widetilde{u}}\right)_{\widetilde{x}} &= \tfrac{\partial}{\partial\widetilde{x}}\textstyle\int_0^{\widetilde{h}} \widetilde{u}\left(\widetilde{x}, \widetilde{y}, \widetilde{t}\right) \mathrm{d}\widetilde{y} \\ &= \widetilde{h}_{\widetilde{x}}\widetilde{u}\Big|^{\widetilde{h}} + \textstyle\int_0^{\widetilde{h}} \left(\widetilde{u}_{\widetilde{x}} + \widetilde{v}_{\widetilde{y}}\right) \mathrm{d}\widetilde{y} - \int_0^{\widetilde{h}} \widetilde{v}_{\widetilde{y}} \mathrm{d}\widetilde{y} \\ &= -\widetilde{h}_{\widetilde{t}}\,, \end{aligned}$$

using $\widetilde{u}_{\widetilde{x}}+\widetilde{v}_{\widetilde{y}}=0$, the bottom boundary condition and the kinematic free surface boundary condition. So

$$\widetilde{h}_{\widetilde{t}}+\left(\widetilde{h}\widetilde{\overline{u}}\right)_{\widetilde{x}}=0\,.$$

From the assumption (8.7) it can be concluded that $\widetilde{v}_{\widetilde{y}}$ is independent of $\widetilde{y}$, since

$$\widetilde{v}_{\widetilde{y}}=-\widetilde{u}_{\widetilde{x}}\quad\text{and}\quad\widetilde{u}=\widetilde{u}\left(\widetilde{x},\widetilde{t}\right)\,.$$

So

$$\widetilde{v}=-\widetilde{u}_{\widetilde{x}}\widetilde{y}=\left(\frac{\widetilde{h}_{\widetilde{t}}+\widetilde{u}\widetilde{h}_{\widetilde{x}}}{\widetilde{h}}\right)\widetilde{y}\,,\tag{8.11}$$

and this shows that the vertical velocity is a linear function of $\widetilde{y}$ (page 147 of Johnson [36]).

Equations (8.9) and (8.10) in terms of the original variables are

$$\begin{aligned}u_t+uu_x+gh_x&=-g\theta-\ddot{q}_1\,,\\ h_t+(hu)_x&=0\,.\end{aligned}$$

This shallow-water model is the simplified version of the more precise new shallow-water model (6.1). Is is asymptotically valid in the limit $\varepsilon\to 0$.

9 Comparison with previous work on rotating SWEs

The first derivation of the SWEs for sloshing in a rotating translating vessel was given by Dillingham [22]. The SWEs are of the same form as (6.3) but the expressions for $a(x,t)$ and $b(x,t)$ are different, and Dillingham uses the average velocity $\overline{u}$ in (1.3). Denote Dillingham's coefficients by $a(x,t)^D$ and $b(x,t)^D$; then (after adapting to the notation here, and noting that Dillingham sets $d_1=0$)

$$\begin{aligned}a(x,t)^D&=g\cos\theta+\dot{\Omega}x-\Omega^2d_2+2\Omega\overline{u}-\ddot{q}_1\sin\theta+\ddot{q}_2\cos\theta\,,\\ b(x,t)^D&=-g\sin\theta+\dot{\Omega}d_2+\Omega^2x-\ddot{q}_1\cos\theta-\ddot{q}_2\sin\theta\,.\end{aligned}\tag{9.1}$$

In Dillingham's notation, $d_2=z_d$. To see the difference with a and b in (4.3) rewrite (9.1)

$$\begin{aligned}a(x,t)^D&=a(x,t)+\Omega^2h+2\Omega\overline{u}\,,\\ b(x,t)^D&=b(x,t)-\dot{\Omega}h-2\Omega h_t\,.\end{aligned}\tag{9.2}$$

In this comparison, the surface velocity is assumed close to the average velocity. In general the two velocities may not be close. The precise difference is quantified in (1.3).

The terms Ω^2h and $\dot{\Omega}h$ are neglected by Dillingham as being small compared with Ω^2d_2 and $\dot{\Omega}d_2$, which is reasonable for large d_2 but not for small d_2. (See Figures 2 and 3 for numerical experiments confirming this observation.) The terms $2\Omega\overline{u}$ and $2\Omega h_t$ are due to Dillingham's neglect of the horizontal Coriolis force ($2\Omega v$) which is not justified. Indeed, if $2\Omega v$ is retained and v is replaced by the approximate surface velocity $\approx -h\overline{u}_x$, then the two formulations are closer.

Since the assumptions in Dillingham [22] are not precise it is not easy to see what error is induced by the neglect of the above terms. One implication of these assumptions

is that the conservation form (6.5) is lost in Dillingham's formulation, and there isn't a variational formulation. We also show some numerical experiments in §12 where the two formulations are compared and clear divergence occurs for large times.

Huang & Hsiung [33] give a derivation of the rotating shallow water equations, but their final equations are almost identical to Dillingham's SWEs. They implicitly use $\overline{u}$ for the velocity field, and their functions are related to a and b in (4.3) by (after identifying U and $\overline{u}$)

$$\begin{aligned} a(x,t)^{HH} &= a(x,t) + 2\Omega\overline{u}\,, \\ b(x,t)^{HH} &= b(x,t) - 2\Omega h_t - \dot{\Omega}h\,. \end{aligned}$$

Comparison with (9.2) shows they include one additional term. However, the critical Coriolis terms are missing. They also formulate the translations relative to the body frame rather than the spatial frame (see discussion in §11). However, within certain parameter regimes the numerical results obtained using the HH SWEs compare very well with the surface SWES (see Figure 11 in §12.2). A review on derivation of HH SWEs is given in technical report [8].

Armenio & La Rocca [12] also use the average horizontal velocity but give a more precise derivation of the SWEs. The derivation of [12] is reviewed in Appendix B. The derivation of [12] leads to the following form for the momentum equation

$$\overline{u}_t + \overline{u}\,\overline{u}_x + a(x,t)^{ALR}h_x = b(x,t;y)^{ALR}\,, \tag{9.3}$$

with

$$\begin{aligned} a(x,t)^{ALR} &= g\cos\theta + \dot{\Omega}(x+d_1) - \Omega^2(h+d_2) + 2\Omega\overline{u}\,, \\ b(x,t;y)^{ALR} &= -g\sin\theta - 2\Omega h\overline{u}_x + \dot{\Omega}(y-h+d_2) + \Omega^2(x+d_1)\,. \end{aligned} \tag{9.4}$$

With appropriate change of notation, this is equation (18) in [12]. Note that the vehicle acceleration $\ddot{\mathbf{q}}$ is absent in this derivation but it can be easily added. Henceforth the pair of equations $h_t + (h\overline{u})_x = 0$ and (9.3) are called the ALR SWEs.

With $\ddot{\mathbf{q}}$ neglected, and assuming $U \approx \overline{u}$, the ALR coefficients relative to a and b in (4.3) are

$$\begin{aligned} a(x,t)^{ALR} &= a(x,t) + 2\Omega\overline{u}\,, \\ b(x,t;y)^{ALR} &= b(x,t) + \dot{\Omega}(y-2h) - 2\Omega(h_t + h\overline{u}_x)\,. \end{aligned}$$

The comparison can be simplified by using the mass equation to eliminate the second term in $a(x,t)^{ALR}$ and the third term in $b(x,t;y)^{ALR}$. After this change the two systems are very close (assuming $U \approx \overline{u}$). The coefficient $b(x,t;y)^{ALR}$ still depends on y. There are a number of choices for y: $y = 0$, $y = \frac{1}{2}h$ (obtained by averaging), $y = h$ and $y = 2h$. The most natural choice is $y = \frac{1}{2}h$ which is obtained by averaging. Another interesting choice is $y = h$. In this case the equations have an interesting variational principle (Alemi Ardakani & Bridges [6]). However, the conservation form is lost unless $y = 2h$ which is not physically reasonable. Henceforth in discussing the ALR SWEs we will use the choice $y = h$.

It is remarkable that the ALR SWEs are very close to the surface equations, when U and $\overline{u}$ are identified, especially since the surface equations have only two assumptions, and the ALR SWEs have four assumptions. Although the two sets of SWEs are similar, there are still two principal advantages to using the surface SWEs: first it is very clear what the assumptions are in the derivation, and secondly, the derivation extends in a straightforward way to the case of three-dimensional rotating shallow-water flow, whereas deriving

the SWEs in 3D with the average velocity is very difficult and not always unambiguous (Alemi Ardakani & Bridges [10]).

10 Numerical algorithm for shallow-water sloshing

Sloshing in shallow water relative to a rotating frame has been simulated numerically using a number of different methods. A number of authors have used Glimm's method to simulate shallow water sloshing (e.g. [22, 43, 55, 54]). Glimm's method is very effective in treating a large number of travelling hydraulic jumps, but the solutions are discontinuous. Armenio points out in the discussion of the paper by Huang & Hsiung [32] that Glimm's method also suffers from a strong mass variation over time in a simulation. Jones & Hulme [37] used Lax-Wendroff, but did not find it to be effective. Lax-Wendroff is explicit with a time step restriction and unacceptably large truncation errors (Abbott [2]). Armenio & La Rocca [12] have used space-time conservation elements, developed by Chang [17], which have excellent conservation properties. They find that the method works very well for the simulation of both standing waves and hydraulic jumps, and the speed of travelling hydraulic jumps is well predicted even for large amplitudes of excitation. Huang & Hsiung [32, 33, 34] have used flux-vector splitting. This method, which is originally due to Steger & Warming [61], involves computing eigenvalues of the Jacobian matrices, and is effective for tracking multi-directional characteristics. Their numerical results are qualitatively in agreement with Dillingham [22].

Our strategy for computing shallow-water sloshing is threefold. We want a method which extends easily to the case of two-horizontal space dimensions. Secondly, we want a method that is both implicit and has some numerical dissipation. Thirdly, we want a method which generalizes easily to the case of coupled vessel-fluid motion. For one horizontal space dimension there are a number of methods that could be used. We first implemented the Preissmann scheme (Abbott [2]) and found it to have excellent properties. The Preissmann scheme is also very effective for transcritical flows (Freitag & Morton [29]. However, there are problems with extending the Preissmann scheme to two horizontal space dimensions (Abbott & Basco [3]).

Instead we use a fully-implicit spatially-centred finite difference scheme which leads to a block tridiagonal coefficient matrix. It is similar to a one-dimensional version of the Abbott-Ionescu scheme and the Leendertse scheme [44] which are both widely used in open channel hydraulics. The representation of waves by this scheme is studied in §4.10 of [2] in one and two horizontal space dimensions.

The scheme has numerical dissipation, but the form of the dissipation is similar to the action of viscosity. The truncation error is of the form of the heat equation and so is strongly wavenumber dependent. Moreover the numerical dissipation follows closely the hydraulic structure of the equations. See the technical report Alemi Ardakani & Bridges [9] for an analysis of the form of the numerical dissipation. The numerical dissipation is helpful for eliminating transients and spurious high-wavenumber oscillation in the formation of travelling hydraulic jumps.

Rewrite the governing equations (6.3) in a form suitable for the scheme,

$$\begin{aligned} h_t + Uh_x + hU_x &= 0\,, \\ U_t + (\alpha(x,t) - \Omega^2 h + 2\Omega U)h_x + (U + 2\Omega h)U_x &= \beta(x,t) + \dot{\Omega} h\,, \end{aligned} \tag{10.1}$$

where α and β are the terms that are independent of h and U,

$$\begin{aligned} \alpha(x,t) &= g\cos\theta + \dot{\Omega}(x+d_1) - \Omega^2 d_2 - \ddot{q}_1\sin\theta + \ddot{q}_2\cos\theta\,, \\ \beta(x,t) &= -g\sin\theta + \dot{\Omega}d_2 + \Omega^2(x+d_1) - \ddot{q}_1\cos\theta - \ddot{q}_2\sin\theta\,. \end{aligned} \tag{10.2}$$

In this scheme all space derivatives are approximated by $3-$point centred difference and time derivatives by forward difference. In order to treat the nonlinearity, an iteration scheme is used. In the first sweep, values of h, U from the previous time step are used. These are then updated and a second sweep is implemented. This procedure is repeated until the previous and current values of h and U are within a prescribed tolerance at all points. Denote the current intermediate values of h, U by $h^\star$ and $U^\star$.

The $x-$interval $0 \le x \le L$ is split into $JJ-1$ intervals of length $\Delta x = \frac{L}{JJ-1}$ and so

$$x_j := (j-1)\Delta x\,, \quad j = 1, \ldots, JJ\,,$$

and

$$h_j^n := h(x_j, t_n) \quad \text{and} \quad U_j^n := U(x_j, t_n)\,,$$

where $t_n = n\Delta t$ with Δt the fixed time step.

The discretization of the equations (10.1) is then

$$\begin{aligned} \frac{h_j^{n+1} - h_j^n}{\Delta t} + U_j^\star \frac{h_{j+1}^{n+1} - h_{j-1}^{n+1}}{2\Delta x} + h_j^\star \frac{U_{j+1}^{n+1} - U_{j-1}^{n+1}}{2\Delta x} &= 0\,, \\ \frac{U_j^{n+1} - U_j^n}{\Delta t} + \left(\alpha_j^{n+1} - (\Omega^{n+1})^2 h_j^\star + 2\Omega^{n+1} U_j^\star\right) \frac{h_{j+1}^{n+1} - h_{j-1}^{n+1}}{2\Delta x} & \\ + \left(U_j^\star + 2\Omega^{n+1} h_j^\star\right) \frac{U_{j+1}^{n+1} - U_{j-1}^{n+1}}{2\Delta x} &= \beta_j^{n+1} + \dot{\Omega}^{n+1} h_j^{n+1}\,, \end{aligned} \tag{10.3}$$

where

$$\alpha_j^n := \alpha(x_j, t_n) \quad \text{and} \quad \beta_j^n := \beta(x_j, t_n)\,.$$

Setting

$$\mathbf{z}_j^n = \begin{pmatrix} h_j^n \\ U_j^n \end{pmatrix},$$

equation (10.3) becomes

$$-\mathbf{A}_j^{n+1}\mathbf{z}_{j-1}^{n+1} + \mathbf{B}^{n+1}\mathbf{z}_j^{n+1} + \mathbf{A}_j^{n+1}\mathbf{z}_{j+1}^{n+1} = \begin{pmatrix} 0 & 1 \\ 1 & 0 \end{pmatrix}\mathbf{z}_j^n + \Delta t\,\beta_j^{n+1}\begin{pmatrix} 1 \\ 0 \end{pmatrix}, \tag{10.4}$$

with

$$\mathbf{A}_j^{n+1} = \frac{\Delta t}{2\Delta x}\begin{bmatrix} \widetilde{\alpha_j^{n+1}} & (U_j^\star + 2\Omega^{n+1}h_j^\star) \\ U_j^\star & h_j^\star \end{bmatrix}, \quad \mathbf{B}^{n+1} = \begin{bmatrix} -\dot{\Omega}^{n+1}\Delta t & 1 \\ 1 & 0 \end{bmatrix}, \tag{10.5}$$

and

$$\widetilde{\alpha_j^{n+1}} = \alpha_j^{n+1} - (\Omega^{n+1})^2 h_j^\star + 2\Omega^{n+1} U_j^\star\,.$$

The equations at $j = 1$ and $j = JJ$ are obtained from the boundary conditions. The only boundary condition at $x = 0$ is $U = 0$. The discrete version of this is

$$U_1^n = 0 \quad \text{and} \quad \frac{U_0^n + U_2^n}{2} = 0\,, \quad \text{for all} \quad n \in \mathrm{N}\,. \tag{10.6}$$

To obtain a boundary condition for h, use the mass equation at $x = 0$

$$h_t + h^\star U_x = 0\,,$$

with discretization

$$\frac{h_1^{n+1} - h_1^n}{\Delta t} + h_1^\star \frac{U_2^{n+1}}{\Delta x} = 0\,. \tag{10.7}$$

Combining (10.6) and (10.7) gives the equation for $j = 1$

$$\mathbf{z}_1^{n+1} + \frac{h_1^\star\,\Delta t}{\Delta x}\begin{bmatrix}0 & 1\\ 0 & 0\end{bmatrix}\mathbf{z}_2^{n+1} = \begin{bmatrix}1 & 0\\ 0 & 0\end{bmatrix}\mathbf{z}_1^n\,. \tag{10.8}$$

Similarly at $x = L$,

$$U_{JJ}^n = 0 \quad \text{and} \quad \frac{U_{JJ-1}^n + U_{JJ+1}^n}{2} = 0\,, \quad \text{for all} \quad n \in \mathrm{N}\,. \tag{10.9}$$

and the discrete mass equation is

$$\frac{h_{JJ}^{n+1} - h_{JJ}^n}{\Delta t} - h_{JJ}^\star \frac{U_{JJ-1}^{n+1}}{\Delta x} = 0\,. \tag{10.10}$$

Combining these two equations gives the discretization at $j = JJ$,

$$-\frac{h_{JJ}^\star\,\Delta t}{\Delta x}\begin{bmatrix}0 & 1\\ 0 & 0\end{bmatrix}\mathbf{z}_{JJ-1}^{n+1} + \mathbf{z}_{JJ}^{n+1} = \begin{bmatrix}1 & 0\\ 0 & 0\end{bmatrix}\mathbf{z}_{JJ}^n\,. \tag{10.11}$$

For fixed $h^\star$ and $U^\star$ the following block linear system of equations is to be solved,

$$\begin{aligned}
\mathbf{z}_1^{n+1} + h_1^\star \mathbf{N}\mathbf{z}_2^{n+1} &= \begin{bmatrix}1 & 0\\ 0 & 0\end{bmatrix}\mathbf{z}_1^n\,,\\
-\mathbf{A}_2^{n+1}\mathbf{z}_1^{n+1} + \mathbf{B}^{n+1}\mathbf{z}_2^{n+1} + \mathbf{A}_2^{n+1}\mathbf{z}_3^{n+1} &= \begin{bmatrix}0 & 1\\ 1 & 0\end{bmatrix}\mathbf{z}_2^n + \Delta t\,\beta_2^{n+1}\begin{pmatrix}1\\ 0\end{pmatrix}\,,\\
-\mathbf{A}_3^{n+1}\mathbf{z}_2^{n+1} + \mathbf{B}^{n+1}\mathbf{z}_3^{n+1} + \mathbf{A}_3^{n+1}\mathbf{z}_4^{n+1} &= \begin{bmatrix}0 & 1\\ 1 & 0\end{bmatrix}\mathbf{z}_3^n + \Delta t\,\beta_3^{n+1}\begin{pmatrix}1\\ 0\end{pmatrix}\,,\\
&\vdots \qquad\quad \vdots\\
-\mathbf{A}_{JJ-1}^{n+1}\mathbf{z}_{JJ-2}^{n+1} + \mathbf{B}^{n+1}\mathbf{z}_{JJ-1}^{n+1} + \mathbf{A}_{JJ-1}^{n+1}\mathbf{z}_{JJ}^{n+1} &= \begin{bmatrix}0 & 1\\ 1 & 0\end{bmatrix}\mathbf{z}_{JJ-1}^n + \Delta t\,\beta_{JJ-1}^{n+1}\begin{pmatrix}1\\ 0\end{pmatrix}\,,\\
-h_{JJ}^\star \mathbf{N}\mathbf{z}_{JJ-1}^{n+1} + \mathbf{z}_{JJ}^{n+1} &= \begin{bmatrix}1 & 0\\ 0 & 0\end{bmatrix}\mathbf{z}_{JJ}^n\,.
\end{aligned}$$

where

$$\mathbf{N} := \frac{\Delta t}{\Delta x}\begin{bmatrix}0 & 1\\ 0 & 0\end{bmatrix}\,.$$

The unknown vector is $\mathbf{Z} := (\mathbf{z}_1, \mathbf{z}_2, \ldots, \mathbf{z}_{JJ-1}, \mathbf{z}_{JJ}) \in \mathbb{R}^{JJ} \times \mathbb{R}^{JJ}$. Its coefficient matrix is a block tridiagonal matrix. It is also diagonally dominant, since the norm of $\mathbf{B}^{n+1}$ is of order 1 and the norm of $\mathbf{A}_j^{n+1}$ is of order Δt when Δx is fixed. For fixed $h^\star$ and $U^\star$ this is just a linear system and can be solved by standard algorithms. We used both MATLAB and FORTRAN in order to double check the results. MATLAB is quicker to program and has a built in block-tridiagonal solver. FORTRAN is more work to program but executes faster. A slight speedup of the algorithm can be obtained by replacing the nonlinear terms $Uh_x + hU_x$ by the linear term $-h_t$ and this modified algorithm is discussed in ALEMI ARDAKANI & BRIDGES [9].

The coefficient matrices in the block-tridiagonal system are dependent upon $h^\star$ and $U^\star$ so an iterative process is added to the solution procedure. At the beginning of a time step $h_j^\star$ is set equal to h_j^n and $U_j^\star = U_j^n$ for each j. Then the linear system is solved, giving new values for $h^\star$ and $U^\star$ which are used to update the coefficient matrices. This process is repeated until $\max_j\{|h_j^\star - h_j^{n+1}| + |U_j^\star - U_j^{n+1}|\}$ is below some tolerance, typically taken to be 10^{-8}. We have not studied the convergence properties of this iteration, but away from criticality and severe hydraulic jumps the convergence is quick (typically 2-5 iterations). Moreover, according to ABBOTT [2] and ABBOTT & BASCO [3], this type of iteration is widely used in the computational hydraulics community.

The initial conditions for the fluid velocity and height at $t = 0$ are typically taken to be

$$U(x, 0) = 0 \quad \text{and} \quad h(x, 0) = h_0\,, \tag{10.12}$$

where h_0 is the still water level.

11 Rigid body motion of the vessel

The fluid vessel is a rigid body free to undergo any motion in the plane. Every rigid body motion in the plane is uniquely determined by $(\mathbf{q}(t), \mathbf{Q}(t))$ where $\mathbf{q}(t)$ is a vector in $\mathbb{R}^2$ and $\mathbf{Q}(t)$ is an orthogonal matrix with unit determinant (O'REILLY [53]). In the plane this reduces to two translations $q_1(t)$ and $q_2(t)$ and an angle $\theta(t)$.

If the translations are zero, then specifying the motion consists of specifying $\theta(t)$, corresponding to roll or pitch motion of the vessel. Here we will restrict attention to harmonic motion of amplitude δ and frequency ω,

$$\theta(t) = \delta \sin(\omega t)\,, \quad \Omega = \dot\theta\,, \quad \dot\Omega = \ddot\theta\,, \tag{11.1}$$

where δ is of order $\varepsilon = h_0/L$. It is not the value of the frequency that is important, but its value relative to the natural frequency. In the limit of shallow water, the natural frequencies of the fluid are

$$\omega_m = \sqrt{g h_0}\frac{m\pi}{L}\,, \quad m \in \mathrm{N}\,. \tag{11.2}$$

In the case of pure translations, $\theta = 0$ and $q_1(t)$ and/or $q_2(t)$ are specified.

The case of mixed rotation/translation requires more care. From the viewpoint of a rigid body, $\mathbf{q}(t)$ here is the absolute translation: *translation of the origin of the body frame* as in Figure 1. However, in ship hydrodynamics spatial translations are relative to the body motion: *translation in the direction of the body axes*: that is; surge, sway and heave. Hence one must be careful in interpreting the literature. For example, DILLINGHAM [22]

uses absolute translation as here, whereas HUANG & HSIUNG [33] and FALTINSEN & TIMOKHA [27] use translations along the body axes. Either choice is correct, but one must be careful in interpretation. For example, in [27], a coupled pitch-surge excitation is proposed of the form (adjusting to the notation here)

$$q_1^{\text{surge}}(t) = A_1 \sin(\omega t)\,, \quad q_2^{heave}(t) = 0 \quad \text{and} \quad \theta(t) = A_2 \cos(\omega t)\,, \tag{11.3}$$

where A_1 and A_2 are specified amplitudes. The surge $q_1^{\text{surge}}(t)$ is along the $x-$axis which is attached to the body. Hence the absolute acceleration vector is

$$\begin{aligned} \ddot{q}_1(t) &= \cos\theta(t)\, \ddot{q}_1^{\text{surge}}(t)\,, \\ \ddot{q}_2(t) &= \sin\theta(t)\, \ddot{q}_1^{\text{surge}}(t)\,, \end{aligned}$$

since in general

$$\begin{pmatrix} \ddot{q}_1 \\ \ddot{q}_2 \end{pmatrix} = \begin{bmatrix} \cos\theta & -\sin\theta \\ \sin\theta & \cos\theta \end{bmatrix} \begin{pmatrix} \ddot{q}_1^{\text{surge}} \\ \ddot{q}_2^{\text{heave}} \end{pmatrix}\,.$$

There is an induced vertical displacement relative to the absolute frame. In other words, to represent a pure pitch-surge excitation of the form (11.3) would require an experiment which specified *both* vertical and horizontal displacements of the vessel *relative to a laboratory frame of reference*.

Therefore the natural approach for comparison with experiments (particularly when both rotation and translation are present) is to specify the absolute translations along with the rotations. On the other hand, we are not aware of any experiments which combine both. The paper of DISIMILE ET AL. [24] indicates that their experimental facility has the capability to produce all 6 degrees of freedom in the forcing, but only planar rotations are reported so far.

When both translations and rotations are specified and are harmonic there is the possibility of two frequencies, resulting in quasiperiodic forcing. The simplest analogous model is that of Duffing's equation with quasiperiodic forcing. This problem has been studied by WIGGINS [66] and he shows that chaos results, and experiments of MOON & HOLMES [48] on quasiperiodic forcing also indicate chaos. In this paper, the simplest coupled forcing is considered, where both frequencies are the same, but the phase differs and results on this are presented in §13.

12 Numerical experiments

Our first numerical experiment is to compare the computations using the surface SWEs with Dillingham's SWEs. In order to facilitate comparison the same numerical method is used for both, with the only difference being the choice of $a(x,t), b(x,t)$ for the surface SWEs and the choice $a(x,t)^D, b(x,t)^D$ for the case of Dillingham's SWEs. Fix data as shown in the first row of Table 1. Then with the initial conditions (10.12) a comparison between the two systems is shown in Figures 2 and 3. A particular value of x is chosen ($x = 0.4\,m$) and the time dependence of $h(x,t)$ at that location is plotted as a function of time.

The results diverge after some time. The error is predominantly amplitude error, but then at larger times, some phase errors appear. $|d_2| = 0.5\,m$ in Figure 2, and $|d_2|$ is 10 times smaller in Figure 3. The larger divergence between the two results when $|d_2|$ is small confirms the prediction based on the analysis of the equations in §9.

Table 1: Input data for the numerical experiments in Figures 2–14. In all cases, $q_1(t) = q_2(t) = 0$ and the initial conditions are $h(x,0) = h_0$ and $U(x,0) = 0$. The first natural frequency ω_1 is listed to two significant figures using (11.2) with $g = 9.81\,m/s^2$.

Figure	L	h_0	d_1	d_2	δ	ω	ω_1	Δx	Δt
	(m)	(m)	(m)	(m)	(rad)	(rad/sec)	(rad/sec)	(m)	(sec)
2	0.5	0.075	-0.25	± 0.5	$\pi/180$	10.77	5.39	0.005	0.005
3	0.5	0.075	-0.25	± 0.05	$\pi/180$	10.77	5.39	0.005	0.005
4	0.5	0.025	-0.25	0.048	varying	varying	3.11	0.005	0.005
5	0.5	0.025	-0.25	0.048	$0.91\pi/180$	3.98	3.11	0.005	0.005
8	0.5	0.05	-0.25	0.048	$0.91\pi/180$	5.05	4.40	0.005	0.005
9	0.5	0.05	-0.25	0.048	$0.91\pi/180$	5.56	4.40	0.005	0.005
10	0.5	0.025	-0.25	0.048	$1.70\pi/180$	3.98	3.11	0.005	0.005
11	1	0.06	-0.5	-0.522	0.067	2.40	2.41	0.005	0.005
12	0.5	0.075	-0.25	varying	$\pi/180$	varying	5.39	0.005	0.005
13,14	0.5	0.075	-0.25	0.0	$\pi/180$	5.0	5.39	0.005	0.005

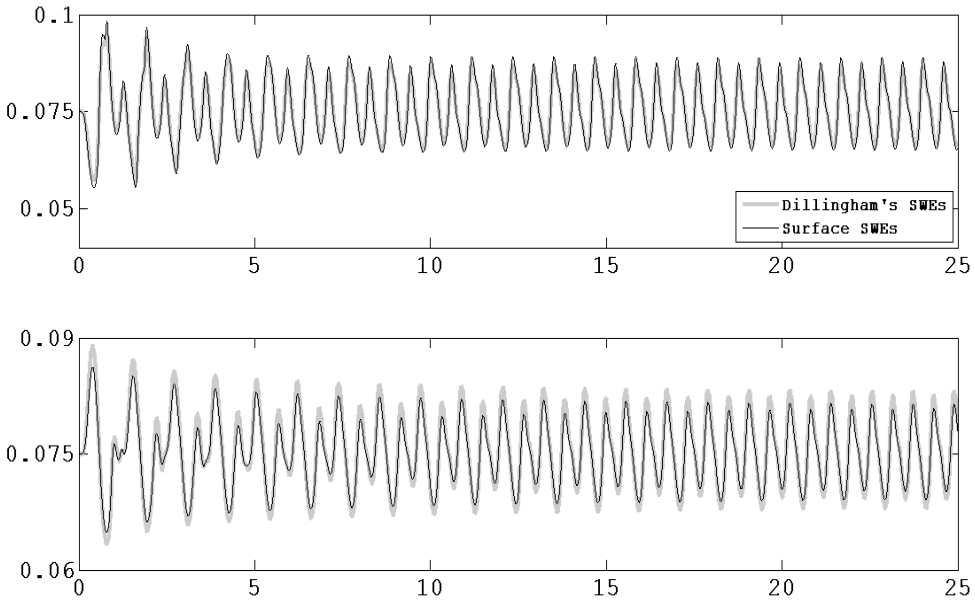

Figure 2: Surface elevation at $x = 0.40\,m$ with parameters listed in Table 1 showing a comparison between the surface SWEs and Dillingham's SWEs. $d_2 = 0.50\,m$ and $d_2 = -0.50\,m$ for upper and lower figures respectively. The horizontal axis is time in *sec* and the vertical axis is wave height in m.

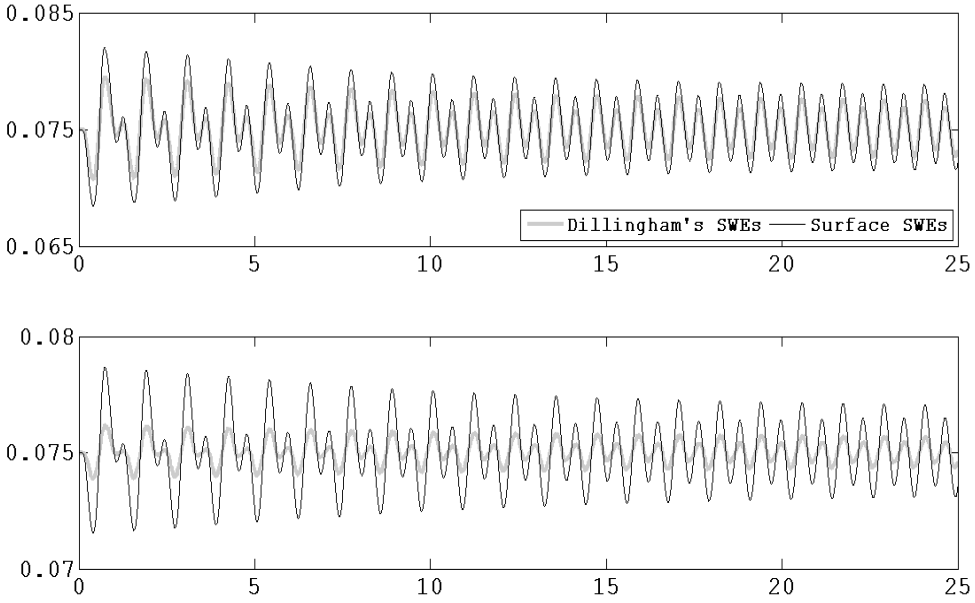

Figure 3: Same as Figure 2 with $d_2 = 0.05\,m$ and $d_2 = -0.05\,m$ for the upper and lower figures respectively.

12.1 Comparison with the ALR SWEs

Armenio & La Rocca [12] present numerical simulations using the ALR SWEs (9.3) and they compare their results with both in house experiments and direct numerical simulations of the two-dimensional flowfield using a marker-and-cell type method including Reynold's averaging (called RANSE in their paper). Here we will compare numerical simulations of the surface SWEs with the ALR SWEs simulations, and by inference also compare with their experiments and RANSE simulations.

[12] point out that the experiments were not able to produce strictly harmonic forcing, and so they used the experimental tank motion as input into the numerics rather than a strict harmonic function. Here we will use a strictly harmonic forcing for the angular motion, and this may affect the comparison.

The two graphs in Figure 4 show the computational results corresponding to Figures 13 and 14 in [12]. The parameter values are listed in the third row of Table 1. The only difference between the upper and lower data sets is the forcing amplitude. It is 0.91^o in lower graph in Figure 4 and 1.7^o in the upper graph. The figure shows the maximum wave height ($|h_{max} - h_{min}|/L$) as a function of the forcing frequency. The natural frequency is approximately π, and that is typically where the maximum amplitude occurs. The comparison is qualitatively good but the slope is much more gentle in these figures. This difference could be due to either the change in forcing, or the effect of transients.

The time dependence of the wave height at a fixed value of x ($x = 0.4\,m$) is plotted in Figure 5. The parameters are the same as in Figure 4 (at the lower forcing amplitude) but with the forcing frequency fixed at $\omega = 3.98\,rad/sec$. Note that there are transient values of the wave height which exceed the steady state (periodic) maximum amplitude.

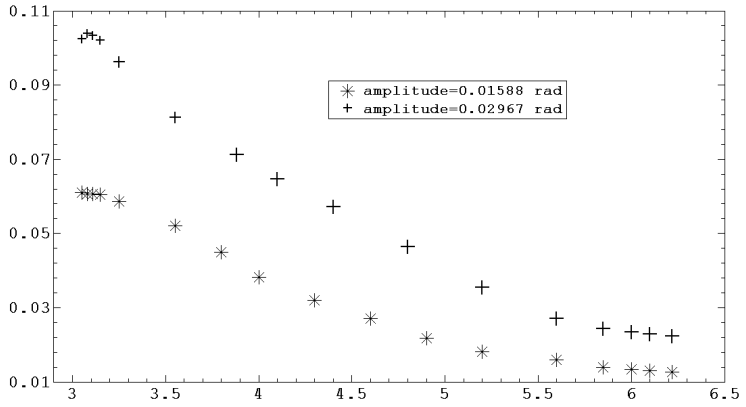

Figure 4: Comparison of the computation with the surface SWEs with Figure 13 and Figure 14 of [12]. The horizontal axis is time in frequency rad/sec and the vertical axis is nondimensional wave height at $x = 0.4m$ in m.

The appearance of large transients and eventual settling down to steady state motion is precisely what occurs in Figure 15 of [12]. This behaviour is consistent with the RANSE simulations although both the RANSE simulations and the experiments show the appearance of additional harmonics. To see what is happening in the transient versus steady state regimes in Figure 5, snapshots of the vessel showing the spatial dependence of the waveheight are shown at a sequence of times in Figures 6 and 7. The initial transient region corresponds to a travelling hydraulic jump, and it settles down to a periodic standing wave.

Figures 8 and 9 show the dramatic difference between forcing near the natural frequency and forcing away from the natural frequency. Figure 8 has parameter values corresponding to Figure 20 in [12]: $h_0/L = 0.10$, $\omega = 5.05\, rad/sec$ (close to resonance) and $\delta = 0.91^o$. The time history of the wave height is shown at $x = 0.40\, m$. The qualitative agreement with Figure 20 in [12] is excellent. However, their RANSE simulations show the presence of several additional wave modes. This comparison is an example where the SWEs capture the principal qualitative properties of the waves but not the detail.

Figure 9 shows a computation with the surface SWEs with parameter values associated with Figure 21 in [12]. Same data as in Figure 8 but with $\omega = 5.56$ rad/sec, so it is away from resonance. In this case the motion is much more regular. Again this simulation compares very well with the SWE simulation in Figure 21 of [12]. In this case the RANSE simulations and the experiments had an additional high frequency component, which gave the appearance of beating.

Figure 10 shows spatial dependence of the wave profiles at parameter values corresponding to Figure 17 in [12]. The agreement between the current simulations and [12] in this case is excellent.

12.2 Comparison with Huang & Hsiung [33]

The SWEs used in [33] are almost the same as Dillingham's. For pure rotation, they have an example with a strong hydraulic jump which provides a good test of a numerical scheme.

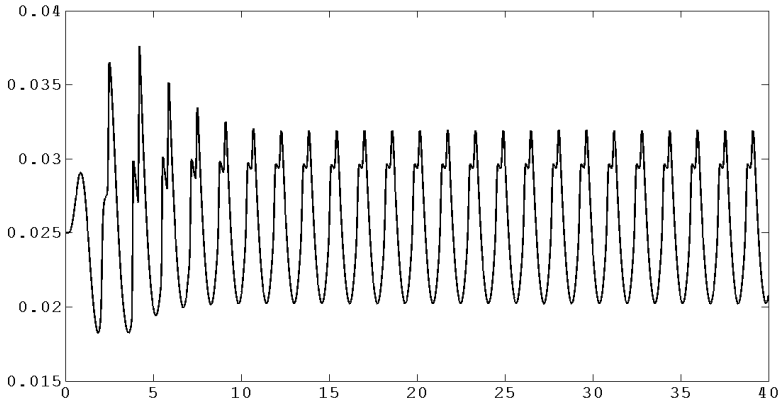

Figure 5: Comparison of the computation with the surface SWEs with Figure 15 of [12]. Data tabulated in Table 1. The horizontal axis is time in *sec* and the vertical axis is wave height in m at $x = 0.4m$.

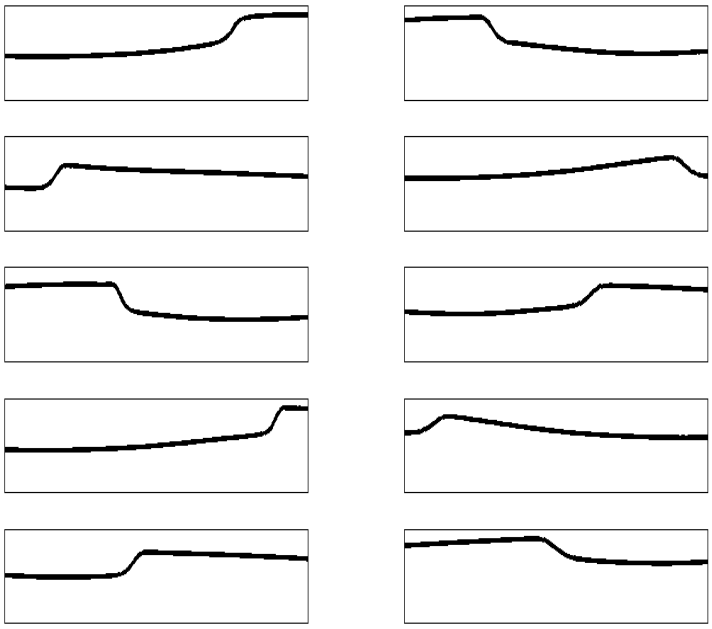

Figure 6: Wave profiles computed using the surface SWEs showing the free surface as a function of x at $t = 2.5\,s$, $t = 3.0\,s$, $t = 3.5\,s$, $t = 4.1\,s$, $t = 4.5\,s$ for the left column from top to bottom and at $t = 5.1\,s$, $t = 5.6\,s$, $t = 6.0\,s$, $t = 6.4\,s$, $t = 6.9\,s$ for the right column from top to bottom. Parameter values the same as in Figure 5.

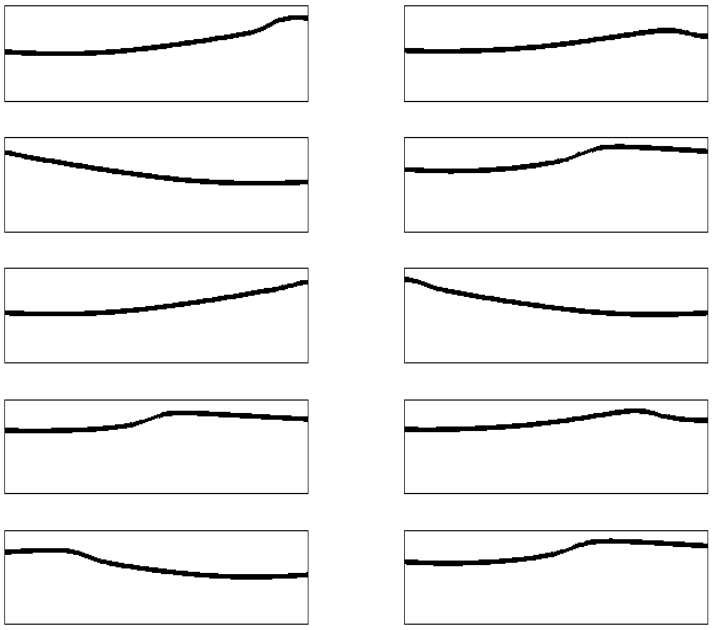

Figure 7: Continuation of Figure 6. Wave profiles computed using the surface SWEs showing the free surface as a function of x. The snapshots are at $t = 9.0\,s$, $t = 9.7\,s$, $t = 10.5\,s$, $t = 10.9\,s$, $t = 11.5\,s$ for the left column from top to bottom and at $t = 12.0\,s$, $t = 12.4\,s$, $t = 12.9\,s$, $t = 13.5\,s$, $t = 14.0\,s$ for the right column from top to bottom.

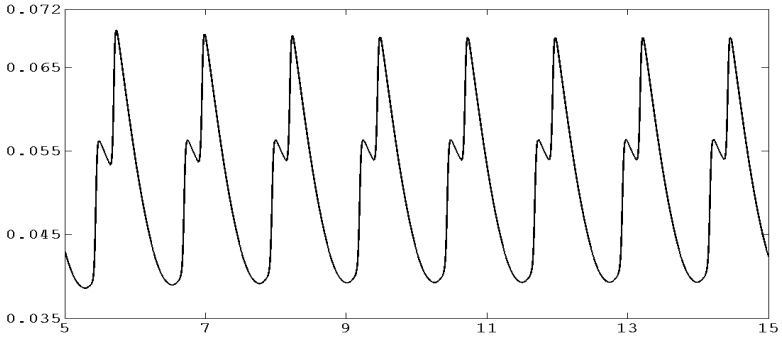

Figure 8: Comparison of the computation with the surface SWEs with Figure 20 of [12]. Data are $h_0 = L/10$, $\omega = 5.05\,rad/sec$ and $\delta = 0.91^o$. The forcing frequency is very close to the natural frequency. The horizontal axis is time in sec and the vertical axis is wave height in m at $x = 0.4m$.

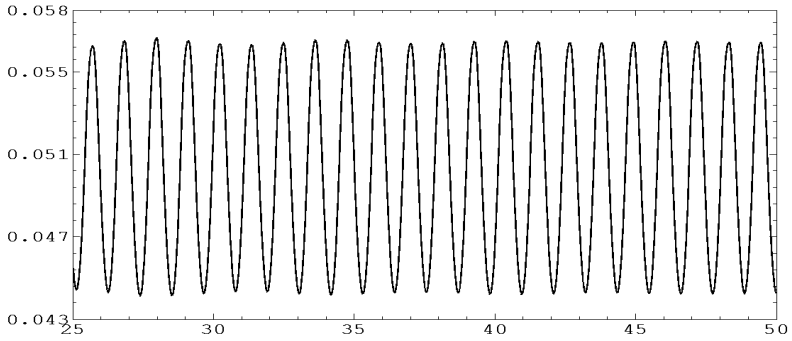

Figure 9: Comparison of the computation with the surface SWEs with Figure 21 of [12]. The data are $h_0 = L/10$, $\omega = 5.56\, rad/sec$ (away from natural frequency), $\delta = 0.91^o$. The horizontal axis is time in sec and the vertical axis is wave height in m at $x = 0.4m$.

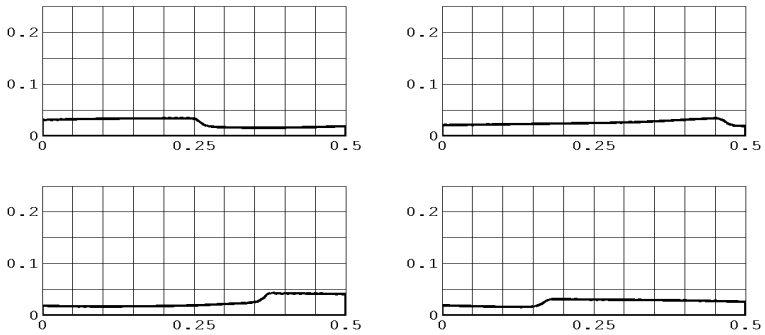

Figure 10: Comparison of the computation with the surface SWEs with Figure 17 of [12]. Data tabulated in Table 1.

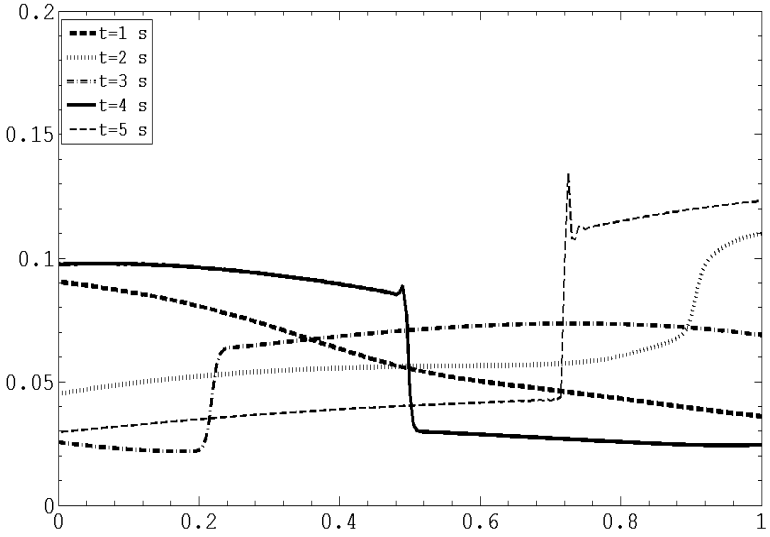

Figure 11: Comparison of the numerics based on the surface SWEs with Figure 6 of [33]. The horizontal axis is x in m and the vertical axis is water depth in m.

Figure 11 shows a simulation using the surface SWEs with parameter values as in Figure 6 of [33]. The frequency is very close to the first natural frequency ($\omega_1 \approx 2.41\, rad/sec$) and, as is typically the case for forcing near the natural frequency, a travelling hydraulic jump forms. The numerics captures the travelling hydraulic jump very well. Surprisingly the results also are close to those of [33], particularly the phase, although the amplitudes differ especially for later times.

12.3 Effect of centre of rotation

An advantage of the SWEs over the full equations is that parametric studies can be carried out quickly. Here an example is shown of the effect of change of the centre of rotation. Suppose the vessel is forced to rotate about a point which lies on the vertical line through the centroid; that is $d_1 = -\frac{1}{2}L$ and d_2 can vary. Taking parameter values as indicated in Table 1, Figure 12 shows the nondimensional wave height at $x = 0.40\, m$ versus d_2, plotted for different frequencies. The principal trend is that when the centre of rotation is below the tank bottom the response is higher and the farther below the larger the amplitude. Hence tanks on the deck of a ship will have greater response than tanks below deck (other parameters being equal), and tanks below the centre of gravity will in general be more stable.

Pantazopoulos [55] shows numerical results including the effect of centre of rotatation (see Figure 6 in Pantazopoulos [55] and Figure 29 in Pantazopoulos [54]). His results show monotone increase of amplitude with d_2. For most frequency values the results in Figure 12 are in qualitative agreement with [55]. However, a new phenomena shows up here when the forcing frequency is at approximately the second natural frequency (the lowest curve in Figure 12), where initially there is a decrease and then increase.

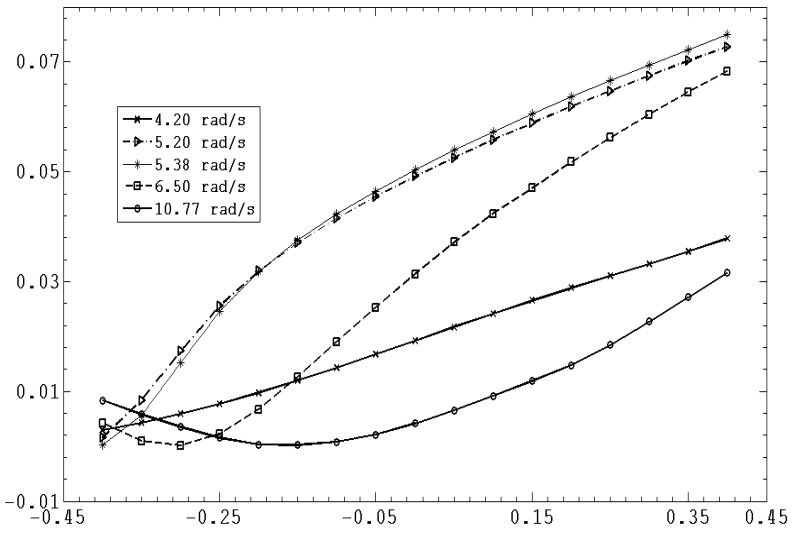

Figure 12: Computed nondimensional wave height versus the center of rotation for different frequencies for the surface SWEs with parameters $\delta = 1.0°$, $L = 0.5\,m$ and $h_0 = 0.075\,m$. The first natural frequency is $\omega_1 \approx 5.38\,rad/sec$. The horizontal axis is d_2 in m and the vertical axis is nondimensional wave height in m at $x = 0.25m$.

12.4 Courant and Froude numbers

The Courant number is important for the numerical propagation of waves (Abbott & Basco [3]). It is optimal, even for an implicit scheme, to operate with a Courant number unity, where the phase and amplitude errors are the smallest. Sloshing is a severe test of this requirement because of the change of direction of the flow. An example to illustrate this is shown in Figure 13. The local Courant number is

$$\mathsf{Cr}(x,t) := \frac{\Delta t}{\Delta x}|U(x,t)|\,.$$

The Courant number is seen to have a rather significant variation over time and space. Nevertheless, the computations using the SWEs seem to capture the qualitative properties of the waves.

With space-time dependent SWEs, the concept of criticality is not precise. But as noted in §6.2 one can define a notion of criticality as the values of parameters at which the Jacobian vanishes (i.e. equation (6.8)). Based on this definition, the critical Froude number is the right hand side of (6.8). When $\theta = 0$, the critical Froude number is unity. For illustration, Figure 14 shows the variation of the critical Froude number as a function of x at various values of time. In this case the variation with x is almost linear, but note that the critical Froude number can exceed unity at some values of x and t. The parameter values are the same as in Figure 13.

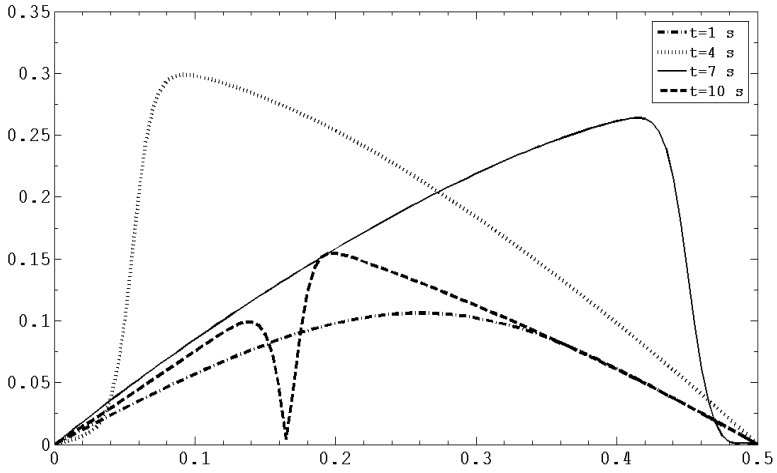

Figure 13: Local Courant number versus x at different values of time. Data tabulated in Table 1. The horizontal axis is x in m and the vertical axis is Courant number.

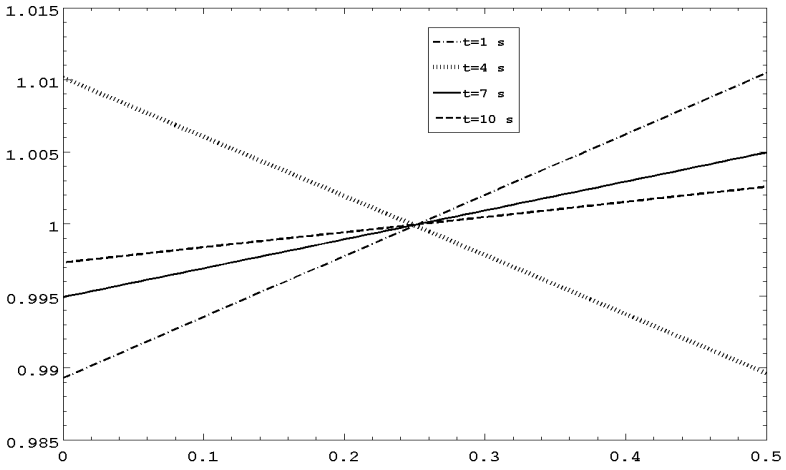

Figure 14: Critical Froude number (right-hand side of (6.8)) versus x at different t. Data tabulated in Table 1. The horizontal axis is x in m and the vertical axis is Froude number squared.

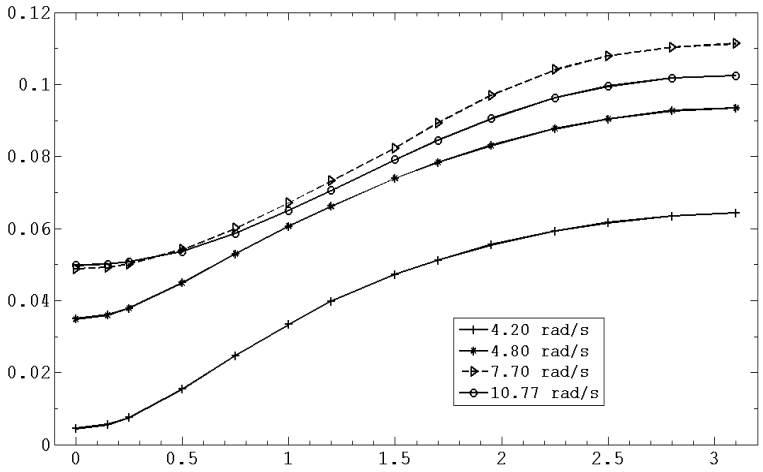

Figure 15: Computed nondimensional wave height ($|h_{max}-h_{min}|/L$) versus the phase shift for different frequencies for the surface SWEs with parameters $\delta = 0.035$, $\theta_0 = 0.5\,rad$, $L = 0.5\,m$, $h_0 = 0.075\,m$, $d_1 = -0.25\,m$, $d_2 = 0.1\,m$, $\Delta x = 0.005\,m$ and $\Delta t = 0.005\,s$. The horizontal axis is θ_1 in rad and the vertical axis is nondimensional wave height at $x = 0.25m$.

13 Coupled surge–pitch forcing

Coupled surge-pitch, or surge-pitch-heave forcing is easily modeled with the surface SWEs. In this section results illustrating the coupled surge-pitch motion are presented. For simplicity the surge and pitch forcing are chosen to be harmonic with the same frequency but out of phase, and the amplitude of the two is the same order of magnitude. The rotation is

$$\theta(t) = \delta\theta_0 \sin(\omega t + \theta_1)\,, \quad 0 \le \theta_1 < \pi\,,$$

and horizontal translation is

$$q_1(t) = \delta L \sin(\omega t)\,.$$

The parameters are fixed at

$$\begin{aligned} \delta &= 0.035\,, \quad \theta_0 = 0.5 \text{ rad}\,, \\ L &= 0.5\,m\,, \quad h_0 = 0.075\,m\,, \quad d_1 = -0.25\,m\,, \quad d_2 = 0.1\,m\,, \end{aligned}$$

and the discretization parameters are $\Delta x = 0.005\,m$ and $\Delta t = 0.005\,s$. Figure 15 shows computed nondimensional wave height ($|h_{max} - h_{min}|/L$) versus the phase shift for different frequencies for the surface SWEs. The maximum response is when the pitch and surge forcing are 180^o out of phase.

Snapshots of the fluid motion at a sequence of times are shown in Figure 13. In this figure the parameter values are

$$\begin{aligned} \delta &= 0.244346\,, \quad \theta_0 = 0.5\,rad\,, \quad \omega = 5.0\,rad/sec\,, \quad \theta_1 = \tfrac{\pi}{6}\,rad\,, \\ L &= 0.5\,m\,, \quad h_0 = 0.15\,m\,, \quad d_1 = -0.25\,m\,, \quad d_2 = 0.0\,m\,, \end{aligned} \tag{13.1}$$

and the numerical parameters are $\Delta x = 0.005\,m$ and $\Delta t = 0.005\,s$. In these simula-

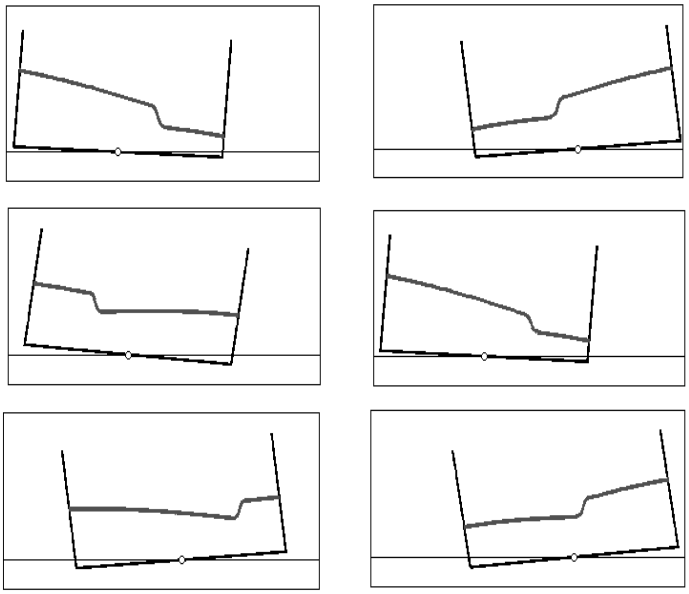

Figure 16: Snapshots of rigid body motion with interior fluid sloshing for coupled surge-pitch motion, with parameter values given in (13.1). The snapshots are at $t = 2.30\,s$, $t = 2.85\,s$ for the first row from left to right, $t = 3.30\,s$, $t = 3.55\,s$ for the second row from left to right, and $t = 3.85\,s$, $t = 4.0\,s$ for the third row from left to right.

tions transients have settled down (these figures show the flowfield between 460 and 800 timesteps). Full simulations including earlier and later times have been combined into a video. This and other sloshing videos can be seen at the Surrey sloshing website [1].

14 Sloshing on London Eye

Here we will restrict attention to sloshing in a vessel attached to a ferris wheel of radius r_c that is prescribed to travel along a circular path such that

$$\begin{aligned} q_1(t) &= -r_c\,(\cos\theta_0 - \cos\theta_c)\ , \\ q_2(t) &= r_c\,(\sin\theta_c - \sin\theta_0)\ , \end{aligned} \tag{14.1}$$

where

$$\theta_c = \omega_c t + \theta_0\,,$$

and is prescribed to harmonically rotate with frequency ω and amplitude δ about the suspension point

$$\theta = \delta\,\sin\omega t\,, \quad \Omega = \dot\theta\,, \quad \dot\Omega = \ddot\theta\,. \tag{14.2}$$

It is not the value of the frequency that is important, but its value relative to the natural frequency 11.2).

Set the input data as

$$\begin{aligned} h_0 &= 0.15\,m\,, \quad L = 1\,m\,, \quad \delta = 0.3047\,rad\,, \\ \omega &= \omega_1 = 3.8109\,rad/sec\,, \quad \theta_0 = 0\,rad\,, \quad \omega_c = 0.5\,rad/sec\,, \\ r_c &= 2\,m\,, \quad d_1 = -0.5\,m\,, \quad d_2 = -0.60\,m\,, \quad \Delta t = 0.01\,sec\,, \\ \Delta x &= 0.01\,m\,. \end{aligned}$$

Then with the initial conditions (10.12) Figure 17 shows the formation and propagation of a travelling hydraulic jump at a sequence of times when the tank is rotating about the suspension point harmonically with the forcing frequency near the first natural frequency of the fluid. This example shows the consistency between the numerical results and the theoretical conclusion of §7 which states that the roll/pitch motion should be an order of magnitude smaller than **q**-translations in order to avoid large fluid motions that would violate (**SWE-1**) and (**SWE-2**).

For the second numerical experiment set the input data as

$$\begin{aligned} h_0 &= 0.15\,m\,, \quad L = 1\,m\,, \quad \delta = 0.15056\,rad\,, \\ \omega &= \omega_2 = 7.6218\,rad/sec\,, \quad \theta_0 = 0\,rad\,, \quad \omega_c = 0.5\,rad/sec\,, \\ r_c &= 2\,m\,, \quad d_1 = -0.5\,m\,, \quad d_2 = -0.60\,m\,, \quad \Delta t = 0.01\,sec\,, \\ \Delta x &= 0.01\,m\,. \end{aligned}$$

Figure 18 shows the snapshots of the rigid-body with the interior fluid sloshing when the frequency of rotation about the suspension point is near the second natural frequency of the fluid which causes the appearance of additional harmonics in the generated wave shape.

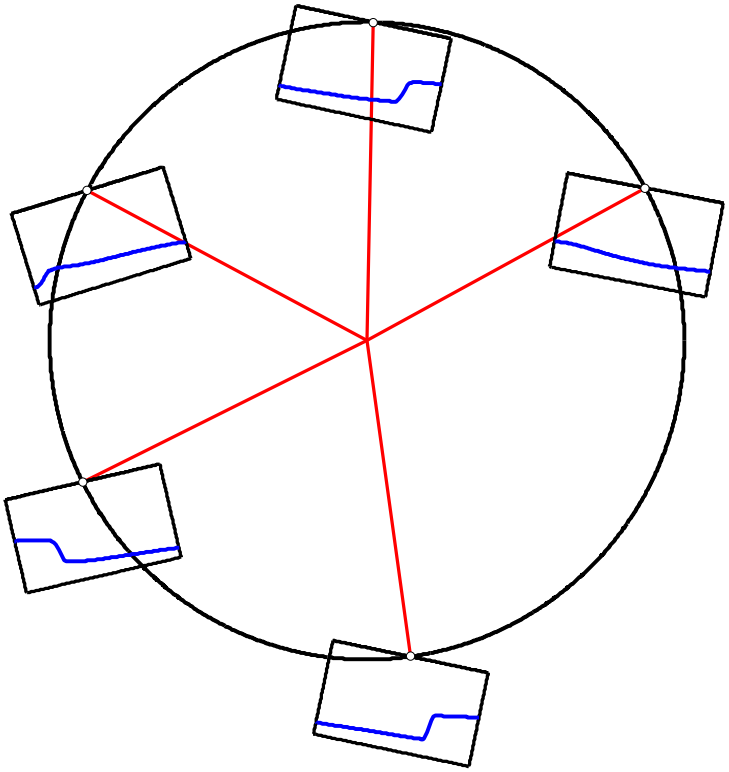

Figure 17: Snapshots of a rigid-body with interior fluid sloshing at a sequence of times. The snapshots in a counterclockwise order are at $t = 1\,sec$, $t = 3.1\,sec$, $t = 5.3\,sec$, $t = 7.2\,sec$ and $t = 9.7\,sec$.

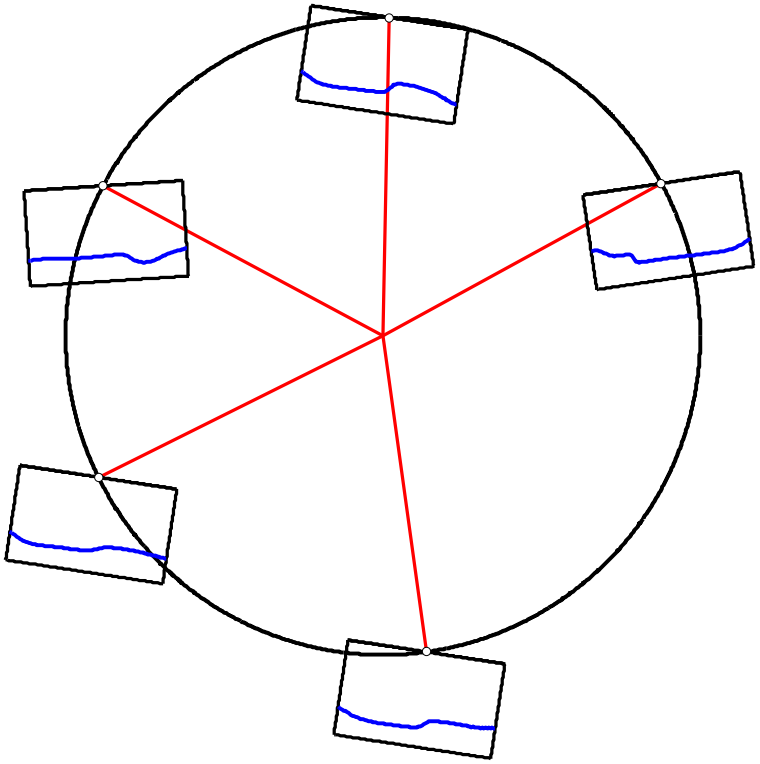

Figure 18: Snapshots of a rigid-body with interior fluid sloshing when $\omega = \omega_2$.

15 Concluding remarks

The starting point of this paper was the surface equations for sloshing in a vessel undergoing rigid body motion in the plane. These equations improve on previous shallow water equations for sloshing in that the vessel motion is exact and there are only two assumptions on the fluid motion. They show how the breaking criterion of Penney-Price-Taylor arises, how surface tension affects the SWEs, and are amenable to numerical simulation. The advantage of restricting to shallow water flow (rather than the full two-dimensional equations) is that numerical imulations of the SWEs are much faster.

Remarkably, all these properties carry over to the case of shallow water sloshing in three dimensions. In Alemi Ardakani & Bridges [10] the surface equations for shallow water sloshing in a vessel undergoing an arbitrary rigid body motion in three dimensions are derived. The motion of the vessel is exact and the only approximations are on the fluid motion, again requiring only two natural hypotheses on the surface vertical velocity and acceleration, generalising (1.9).

In this paper the motion of the vessel has been prescribed. The vessel motion can also be determined by solving the rigid-body equations coupled to the fluid motion. The dynamically coupled problem is studied in [7, 6].

As an example of the coupled problem, consider for simplicity pure horizontal translation of the vessel ($q_2 = \theta = 0$). The exact equation for the dynamically-coupled motion of a vessel of dry mass m_s and spring constant ν with the fluid is

$$\frac{d}{dt}\left(\int_0^L \int_0^h \rho u(x,y,t)\,\mathrm{d}y\mathrm{d}x + (m_s + m_f)\dot{q}_1\right) + \nu q_1 = 0\,,$$

where $m_f = \rho h_0 L$ is the fluid mass. A derivation of this equation is given in [7]. Now, approximate the horizontal momentum by a shallow water model

$$\frac{d}{dt}\left(\int_0^L \rho h U(x,t)\,\mathrm{d}x + (m_s + m_f)\dot{q}_1\right) + \nu q_1 = 0\,.$$

Then using the momentum equation with $q_2 = \theta = 0$ this equation can be reduced to

$$m_s\ddot{q}_1 + \nu q_1 = \tfrac{1}{2}\rho g(h(L,t)^2 - h(0,t))^2\,, \tag{15.1}$$

which is Cooker's equation (Cooker [21]). Solution of the coupled problem, where $q_1(t)$ is determined from (15.1) rather than specified, leads to very different dynamics. The natural frequencies change and the dynamic coupling can mollify the fluid motion or enhance it. Numerical simulation of the coupled problem (6.3) and (15.1) is reported in Alemi Ardakani & Bridges [7]. The full dynamically coupled problem including rotation is studied in Alemi Ardakani [5].

— Appendix —

A Conservation form of the rotating SWEs

The sloshing equations (6.3) can be written in conservation form when surface tension is neglected. This property is surprising since neither Dillingham's SWEs, HH SWEs, or the ALR SWEs have this property.

Let

$$\begin{aligned} R &= \tfrac{1}{2}U^2 + a(x,t)(h+d_2) + \tfrac{1}{2}\Omega^2(h+d_2)^2 \\ &\quad + gx\sin\theta - \tfrac{1}{2}\Omega^2(x+d_1)^2 + (\ddot{q}_1\cos\theta + \ddot{q}_2\sin\theta)x\,. \end{aligned} \tag{A-1}$$

Then the $x-$momentum equation (6.3) can be written in the conservation form

$$(U - 2\Omega(h+d_2))_t + R_x = 0.$$

The mass equation in (6.3) is already in conservation form. However, there is even more structure to these equations. The function R is the derivative of another function with respect to h. Call this function $E(h,U)$. Expand R,

$$\begin{aligned} R &= \tfrac{1}{2}U^2 + g(h+d_2)\cos\theta + gx\sin\theta + \dot{\Omega}(x+d_1)(h+d_2) - \tfrac{1}{2}\Omega^2(x+d_1)^2 \\ &\quad - \tfrac{1}{2}\Omega^2(h+d_2)^2 + (-\ddot{q}_1\sin\theta + \ddot{q}_2\cos\theta)(h+d_2) + (\ddot{q}_1\cos\theta + \ddot{q}_2\sin\theta)x\,, \end{aligned}$$

and integrate $\frac{\partial E}{\partial h} = R$, giving the expression (6.7). Then

$$R = \tfrac{\partial E}{\partial h} \quad \text{and} \quad hU = \tfrac{\partial E}{\partial U}\,, \tag{A-2}$$

and the governing equations are

$$\tfrac{\partial h}{\partial t} + \tfrac{\partial}{\partial x}\left(\tfrac{\partial E}{\partial U}\right) = 0,$$

and

$$\tfrac{\partial}{\partial t}\left(U - 2\Omega(h+d_2)\right) + \tfrac{\partial}{\partial x}\left(\tfrac{\partial E}{\partial h}\right) = 0.$$

Further define the momentum by (6.6). Then the governing equations take the form

$$\tfrac{\partial}{\partial t}(\nabla I) + \tfrac{\partial}{\partial x}(\nabla E) = 0\,, \tag{A-3}$$

where the gradient consists of derivatives with respect to h and U.

This form of the equations captures an important property of the classical shallow water equations. Benjamin & Bowman [13] show that the classical shallow water equations can be expressed in terms of the energy E and momentum I,

$$E = \tfrac{1}{2}hu^2 + \tfrac{1}{2}gh^2 \quad \text{and} \quad I = hu\,.$$

Then with $\nabla E = (gh + \frac{1}{2}u^2, uh)$ and $\nabla I = (u, h)$, the classical SWEs are recovered by substituting E and I into the form (A-3).

B Derivation of Armenio & La Rocca's (1996) SWEs

In the derivation of Armenio & La Rocca [12], the mean velocity (1.3) is used and so the mass equation is exact. In this appendix a review of the derivation of the SWE momentum equation due to [12] is given. The reduction of the momentum equations proceeds as follows. The translation accelerations $\ddot{\mathbf{q}}$ are neglected since they do not affect the derivation. The starting point of the ALR derivation is the momentum equations

$$\begin{aligned} \frac{Du}{Dt} + \frac{1}{\rho}\frac{\partial p}{\partial x} &= -g\sin\theta + 2\Omega v + \dot{\Omega}(y+d_2) + \Omega^2(x+d_1)\,, \\ \frac{Dv}{Dt} + \frac{1}{\rho}\frac{\partial p}{\partial y} &= -g\cos\theta - 2\Omega u - \dot{\Omega}(x+d_1) + \Omega^2(y+d_2)\,, \end{aligned} \tag{B-1}$$

The first assumption is to neglect the vertical acceleration

$$\frac{Dv}{Dt} \approx 0\,. \tag{**ALR-1**}$$

The vertical momentum equation then reduces to

$$\frac{1}{\rho}\frac{\partial p}{\partial y} = -g\cos\theta - 2\Omega u - \dot{\Omega}(x+d_1) + \Omega^2(y+d_2)\,,$$

Integrate this equation over the entire depth

$$\frac{1}{\rho}p(x,y,t)\bigg|^h - \frac{1}{\rho}p(x,0,t) = -gh\cos\theta - 2\Omega\int_0^h u\,\mathrm{d}y - \dot{\Omega}(x+d_1)h + \tfrac{1}{2}\Omega^2(h^2+2hd_2)\,.$$

Applying the dynamic free surface boundary condition, and neglecting surface tension, gives an expression for the pressure field at $y=0$

$$\frac{1}{\rho}p(x,0,t) = gh\cos\theta + 2\Omega h\overline{u} + \dot{\Omega}(x+d_1)h - \tfrac{1}{2}\Omega^2(h^2+2hd_2)\,.$$

Now consider the $x-$momentum equation in (B-1). To simplify this equation two assumptions are invoked

$$2\Omega v \approx 0\,, \tag{**ALR-2**}$$

and

$$\frac{1}{\rho}\frac{\partial p}{\partial x} \quad \text{in the } x-\text{momentum equation is evaluated at } y=0\,. \tag{**ALR-3**}$$

With these assumptions the $x-$momentum equation simplifies to

$$\frac{Du}{Dt} + \frac{1}{\rho}\frac{\partial p}{\partial x}\bigg|_{y=0} = -g\sin\theta + \dot{\Omega}(y+d_2) + \Omega^2(x+d_1)\,,$$

with

$$\frac{1}{\rho}\frac{\partial p}{\partial x}\bigg|_{y=0} = gh_x\cos\theta + 2\Omega(h\overline{u})_x + \dot{\Omega}h + \dot{\Omega}(x+d_1)h_x - \Omega^2(h+d_2)h_x\,.$$

However, the system is still not closed. One additional assumption is required

$$\frac{Du}{Dt} \approx \overline{u}_t + \overline{u}\,\overline{u}_x\,. \tag{**ALR-4**}$$

With this hypothesis, the $x-$momentum equation becomes (9.3) with coefficients (9.4).

The first two assumptions (**ALR-1**)-(**ALR-2**) are analogues of the ones used in the derivation of the surface equations in §3. It is difficult to quantify the error in assumption (**ALR-3**). The error in Assumption (**ALR-4**) can be clarified however, since

$$\frac{1}{h}\int_0^h \frac{Du}{Dt}\,\mathrm{d}y - \overline{u}_t - \overline{u}\,\overline{u}_x = \frac{1}{h}\frac{\partial}{\partial x}\left(\int_0^h u^2\,\mathrm{d}y - h\overline{u}^2\right).$$

Hence the error is small if the the right-hand side of this expression is small. A sufficient condition for neglect is when the depth-averaged velocity squared is close to the square of the depth-averaged velocity.

C Vertical accelerations and the highest standing wave

One of the interesting features of the exact surface equation for the horizontal surface velocity is the way that the vertical acceleration appears. Define

$$a^L(x,t) = g + \left.\frac{Dv}{Dt}\right|^h = -\left.\frac{\partial p}{\partial y}\right|^h. \tag{C-1}$$

A condition proposed by Penney & Price [56] for the limiting periodic standing wave is $a^L = 0$. They argued that – in the absence of surface tension – the pressure just inside the liquid near the surface for a standing wave must be positive or zero and consequently at the surface $\frac{\partial p}{\partial y} \leq 0$ which is equivalent to $a^L \geq 0$. When this condition is violated then the standing wave should cease to exist.

Experiments of Taylor [62] confirmed the importance of a^L in determining the highest wave. Numerical calculations of Saffmann & Yuen [60] also found that $a^L \approx 0$ for standing waves near breaking. In their discussion of breaking mechanisms for sloshing waves, the authors of Royon-Lebeaud et al. [58] remark that a destabilization of a standing wave first appears when the wave front acceleration exceeds the acceleration of gravity. Okamura [52] has computed large amplitude standing waves with crest accelerations up to $-0.9998\,g$, with a^L tending to zero at the crest as the limiting standing wave is approached.

The property that the vertical acceleration tends to $-g$ as the highest wave is approached is distinctly different from the case of Stokes progressive waves where the vertical acceleration at the crest tends to $-\frac{1}{2}g$ as the Stokes limiting wave is approached Longuet-Higgins [45]. Okamura [52] also shows that the crest acceleration provides a better parameterization than wave height for very steep waves. In his study of vertical jets emitted by *unsteady* standing waves, Longuet-Higgins [46] found vertical accelerations exceeding $-10g$.

Reformulate the governing equations around the function a^L. The exact governing equations for (h, U, V) are

$$\begin{aligned} &h_t + U\,h_x = V\,,\\ &U_t + U\,U_x + a^L\,h_x = \sigma\kappa_{xx}\,,\\ &V_t + U\,V_x + g = a^L\,. \end{aligned} \tag{C-2}$$

The latter equation follows by noting that

$$\begin{aligned} V_t + UV_x &= v_t\Big|^h + v_y\Big|^h h_t + U\left(v_x\Big|^h + v_y\Big|^h h_x\right) \\ &= (v_t + uv_x + vv_y)\Big|^h + (h_t + Uh_x - V)v_y\Big|^h \\ &= \tfrac{Dv}{Dt}\Big|^h = a^L - g\,. \end{aligned}$$

The equations (C-2) are not closed – unless a^L is given.

Taking the limit $a^L \to 0$ and neglecting surface tension, the equation for U reduces to the inviscid Burger's equation $U_t + UU_x = 0$ which has solutions that blow up in finite time. Pomeau et al. [57] argue that this singularity is related to wave breaking (Bridges [15]). Hence the Penney-Price-Taylor criterion is indeed a limiting condition for standing waves.

By combining the $x-$momentum equation (neglecting surface tension) with the mass equation (assuming $|V + hU_x|$ is small) gives

$$h_t + (hU)_x = 0 \quad \text{and} \quad U_t + UU_x + a^L h_x = 0\,.$$

In this case the limit $a^L \to 0$ is similar to the high Froude number limit of classical shallow water theory, and this limit produces a range of exotic solutions Edwards et al. [25].

One can derive a form of energy equation for (C-2) when $\sigma = 0$,

$$\mathcal{E}_t + U\,\mathcal{E}_x = a^L h_t\,, \quad \mathcal{E} := \tfrac{1}{2}(U^2 + V^2) + gh\,.$$

If $a^L \approx 0$ is the appropriate condition for wave breaking in a stationary vessel, it suggests that the appropriate condition for wave breaking in a rotating translating vessel is

$$\frac{Dv}{Dt}\Big|^h + g\cos\theta + \dot\Omega(x + d_1) - \Omega^2(h + d_2) - \ddot q_1 \sin\theta + \ddot q_2 \cos\theta \approx 0\,.$$

References

[1] `http://personal.maths.surrey.ac.uk/st/T.Bridges/SLOSH/`

[2] M.B. Abbott. *Computational Hydraulics: Elements of the Theory of Free-Surface Flows*, London: Pitman Publishers (1979).

[3] M.B. Abbott & D.R. Basco. *Computational Fluid Dynamics: An Introduction for Engineers*, Essex, UK: Longman Scientific (1989).

[4] B.H. Adee & I. Caglayan. *The effects of free water on deck on the motions and stability of vessels*, In Proc. Second Inter. Conf. Stab. Ships and Ocean Vehicles, pp. 413–426. Berlin: Springer (1982).

[5] H. Alemi Ardakani. *Rigid-body motion with interior shallow-water sloshing*, PhD Thesis, University of Surrey (2010).

[6] H. Alemi Ardakani & T.J. Bridges. *Coupled roll motion of a liquid-tank system with shallow water*, (in preparation, 2010).

[7] H. Alemi Ardakani & T.J. Bridges. *Dynamic coupling between shallow water sloshing and horizontal vehicle motion*, Europ. J. Appl. Math. (in press, 2010).

[8] H. Alemi Ardakani & T.J. Bridges. *Review of the Huang-Hsiung rotating two-dimensional shallow-water equations*, Tech. Rep., Department of Mathematics, University of Surrey (2009).

[9] H. Alemi Ardakani & T.J. Bridges. *Shallow water sloshing in rotating vessels: details of the numerical algorithm*, Tech. Rep., Department of Mathematics, University of Surrey (2009).

[10] H. Alemi Ardakani & T.J. Bridges. *Shallow-water sloshing in rotating vessels undergoing prescribed rigid-body motion in three dimensions*, J. Fluid Mech. (in press, 2010).

[11] H. Alemi Ardakani & T.J. Bridges. *The Euler equations in fluid mechanics relative to a rotating-translating reference frame*, Technical Report, Department of Mathematics, University of Surrey (2010).

[12] V. Armenio & M. La Rocca. *On the analysis of sloshing of water in rectangular containers: numerical study and experimental validation*, Ocean Eng. **23** 705–739 (1996).

[13] T.B. Benjamin & S. Bowman. *Discontinuous solutions of one-dimensional Hamiltonian systems*, Proc. Royal Soc. London A **413** 263–295 (1987).

[14] J. Billingham. *Nonlinear sloshing in zero gravity*, J. Fluid Mech. **464** 365–391 (2002).

[15] T.J. Bridges. *Wave breaking and the surface velocity field for three-dimensional water waves*, Nonlinearity **22** 947–953 (2009).

[16] I. Caglayan & R.L. Storch. *Stability of fishing vessels with water on deck: a review*, J. Ship Research **26** 106–116 (1982).

[17] S.-C. Chang. *The method of space-time conservation elements and solution element – a new approach for solving the Navier-Stokes and Euler equations*, J. Comp. Phys. **119** 295–324 (1995).

[18] B.-F. Chen. *Viscous fluid in tank under coupled surge, heave and pitch motions*, ASCE J. Waterways, Port, Coastal & Ocean Eng. **131** 239–256 (2005).

[19] W. Chester. *Resonant oscillations of water waves. I. theory*, Proc. Royal Soc. London A **306** 5–22 (1968).

[20] W. Chester & J.A. Bones. *Resonant oscillations of water waves. II. experiment*, Proc. Royal Soc. London A **306** 23–39 (1968).

[21] M.J. Cooker. *Water waves in a suspended container*, Wave Motion **20** 385–395 (1994).

[22] J. Dillingham. *Motion studies of a vessel with water on deck*, Marine Technology **18** 38–50 (1981).

[23] M.W. Dingemans. *Water Wave Propagation Over Uneven Bottoms. Part 2: Nonlinear Wave Propagation*. Singapore: World Scientific (1997).

[24] P.J. Disimile, J.M. Pyles & N. Toy. *Hydraulic jump formation in water sloshing within an oscillating tank*, J. Aircraft **46** 549–556 (2009).

[25] C.M. Edwards, S.D. Howison, H. Ockendon & J.R. Ockendon. *Nonclassical shallow water flows*, IMA J. Applied Math. **73** 137–157 (2007).

[26] O.M. Faltinsen, O.F. Rognebakke, I.A. Lukovsky & A.N. Timokha. *Multidimensional modal analysis of nonlinear sloshing in a rectangular tank with finite water depth*, J. Fluid Mech. **407** 201–234 (2000).

[27] O.M. Faltinsen & A.N. Timokha. *Asymptotic modal approximation of nonlinear resonant sloshing in a rectangular tank with small fluid depth*, J. Fluid Mech. **470** 319–357 (2002).

[28] O.M. Faltinsen & A.N. Timokha. *Sloshing*, Cambridge University Press (2009).

[29] M.A. Freitag & K.W. Morton. *The Preissmann box scheme and its modifications for transcritical flows*, Int. J. Numer. Meth. Engng. **70** 791–811 (2007).

[30] T. Gedeon, H. Kokubu, K. Mischaikow & H. Oka. *Chaotic solutions in slowly-varying perturbations of hamiltonian systems with applications to shallow-water sloshing*, J. Dyn. Diff. Eqns. **14** 63–84 (2004).

[31] S.P. Hastings & J.B. McLeod. *On the periodic solutions of a forced second-order equation*, J. Nonlinear Sci. **1** 225–245 (1991).

[32] Z.J. Huang & C.C. Hsiung. *Application of the flux difference splitting method to compute nonlinear shallow water flow on deck*, In the Proc. 9th Int. Workshop on Water Waves and Floating Bodies, Japan, 17-20 April 1994, pp. 83–87, IWWWFB (1994).

[33] Z.J. Huang & C.C. Hsiung. *Nonlinear shallow water flow on deck*, J. Ship Research **40** 303–315 (1996).

[34] Z.J. Huang & C.C. Hsiung. *Nonlinear shallow-water flow on deck coupled with ship motion*. In the Twenty-First Symposium on Naval Hydrodynamics, pp. 220–234, National Academies Press (1997).

[35] R.A. Ibrahim. *Liquid Sloshing Dynamics*, Cambridge University Press (2005).

[36] R.S. Johnson. *A Modern Introduction to the Mathematical Theory of Water Waves*, Cambridge University Press (2001).

[37] A.F. Jones & A. Hulme. *The hydrodynamics of water on deck*, J. Ship Research **31** 125–135 (1987).

[38] T.J. Kaper & S. Wiggins. *A commentary on "The periodic solutions of a forced second-order equation" by S.P. Hastings and J.B. MacLeod*, J. Nonlinear Sci. **1** 247–253 (1991).

[39] J.J. Kobine. *Nonlinear resonant characteristics of shallow fluid layers*, Phil. Trans. Royal Soc. London A **366** 1131–1346 (2008).

[40] M. La Rocca, G. Sciortino & M.A. Boniforti. *A fully nonlinear model for sloshing in a rotating container*, Fluid Dynamics Res. **27** 23–52 (2000).

[41] J. Laranjinha, J.M. Falzarano & C.G. Soares. *Analysis of the dynamical behaviour of an offshore supply vessel with water on deck*, In the Proc. 21st Inter. Conf. Offshore Mechanics and Arctic Eng. (OMAE02), Paper No. OMAE2002-OFT28177, ASME (2002).

[42] S.K. Lee, S. Surendran & G. Lee. *Roll performance of a small fishing vessel with live fish tank*, Ocean Engineering **32** 1873–1885 (2005).

[43] T.H. Lee, Z. Zhou & Y. Cao. *Numerical simulations of hydraulic jumps in water sloshing and water impacting*, ASME J. Fluids Eng. **124** 215–226 (2002).

[44] J. Leendertse. *Aspects of a computational model for long-period water wave propagation*, Tech. Rep. RM-5294-PR. Rand Corporation (1967).

[45] M.S. Longuet-Higgins. *On the form of the highest progressive and standing waves in deep water*, Proc. Royal Soc. London A **331** 445–456 (1973).

[46] M.S. Longuet-Higgins. *Vertical jets from standing waves*, Proc. Royal Soc. London A **457** 495–510 (2001).

[47] Y.K. Lou, T.C. Su & J.E. Flipse. *A nonlinear analysis of liquid sloshing in rigid containers*, Tech. Rep. MA-79-SAC-B0018, Texas A&M University (1980).

[48] F.C. Moon & W.T. Holmes. *Double Poincare sections of a quasi-periodically forced, chaotic attractor*, Phys. Lett. A **111** 157–160 (1985).

[49] R.M. Murray, Z.X. Lin & S.S. Sastry. *A Mathematical Introduction to Robotic Manipulation*, Boca Raton, Florida: CRC Press (1994).

[50] J.R. Ockendon & H. Ockendon. *Resonant surface waves*, J. Fluid Mech. **59** 397–413 (1973).

[51] H. Ockendon, J.R. Ockendon & A.D. Johnson. *Resonant sloshing in shallow water*, J. Fluid Mech. **167** 465–479 (1986).

[52] M. Okamura. *Standing gravity waves of large amplitude in deep water*, Wave Motion **37** 173–182 (2003).

[53] O.M. O'Reilly. *Intermediate Dynamics for Engineers: a Unified Treatment of Newton-Euler and Lagrangian Mechanics*, Cambridge: Cambridge University Press (2008).

[54] M.S. Pantazopoulos. *Numerical solution of the general shallow water sloshing problem*, PhD thesis, University of Washington, Seattle (1987).

[55] M.S. Pantazopoulos. *Three-dimensional sloshing of water on decks*, Marine Technology **25** 253–261 (1988).

[56] W.G. Penney & A.T. Price. *Part II. finite periodic stationary gravity waves in a perfect fluid*, Phil. Trans. Royal Soc. London A **244** 254–284 (1952).

[57] Y. Pomeau, M. Le Berre, P. Guyenne & S. Grilli. *Wave breaking and generic singularities of nonlinear hyperbolic equations*, Nonlinearity **21** T61–T79 (2008).

[58] A. Royon-Lebeaud, E.J. Hopfinger & A. Cartellier. *Liquid sloshing and wave breaking in circular and square-based cylindrical coordinates*, J. Fluid Mech. **577** 467–494 (2007).

[59] P. Ruponen, J. Matusiak, J. Luukkonen & M. Ilus. *Experimental study on the behavior of a swimming pool onboard a large passenger ship*, Marine Technology **46** 27–33 (2009).

[60] P.G. Saffmann & H.C. Yuen. *A note on the numerical computations of large amplitude standing waves*, J. Fluid Mech. **95** 707–715 (1979).

[61] J.L. Steger & R.F. Warming. *Flux-vector splitting of the inviscid gasdynamic equations with application to finite-difference methods*, J. Comp. Phys. **40** 263–293 (1981).

[62] G.I. Taylor. *An experimental study of standing waves*, Proc. Royal Soc. London A **218** 44–59 (1953).

[63] M.P. Tzamtzi & N.D. Kouvakas. *Sloshing control of tilting phases of the pouring process*, Inter. J. Math. Phys. Eng. Sciences **1** 175–182 (2007).

[64] J.H.G. Verhagen & L. van Wijngaarden. *Non-linear oscillations of fluid in a container*, J. Fluid Mech. **22** 737–751 (1965).

[65] S. aus der Wiesche. *Computational slosh dynamics: theory and industrial application*, Comp. Mech. **30** 374–387 (2003).

[66] S. Wiggins, S. *Chaos in the quasiperiodically forced Duffing oscillator*, Phys. Lett. A **124** 138–142 (1987).